

**DESIGN AND ANALYSIS OF HEAT
SINK CONFIGURATIONS FOR
PASSIVE COOLING OF SOLAR
PANELS**

**ISHTIAQ AHMED, 170011048
HOSSAIN AZMAIN FARHIN, 170011045
SAZIEA AFRIN HEME, 170011007**

Submitted in Partial Fulfillment
of the Requirements
for the Degree of.

Bachelor of Science in Mechanical Engineering

**DEPARTMENT OF MECHANICAL AND PRODUCTION
ENGINEERING**

May (2022)

CERTIFICATE OF RESEARCH

This thesis titled "DESIGN AND ANALYSIS OF HEAT SINK CONFIGURATIONS FOR PASSIVE COOLING OF SOLAR PANELS" submitted by ISHTIAQ AHMED (170011048), HOSSAIN AZMAIN FARHIN (170011045) and SAZIEA AFRIN HEME (170011007) has been accepted as satisfactory in partial fulfillment of the requirement for the Degree of Bachelor of Science in Mechanical Engineering.

Supervisor

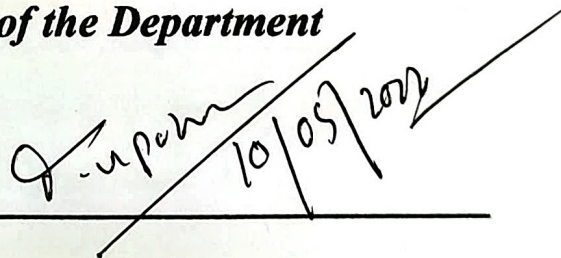


Prof. Dr. Md. Hamidur Rahman

Professor

Department of Mechanical and Production Engineering
(MPE)

Head of the Department



Dr. Md. Anayet Ullah Patwari

Head of the Department

Department of Mechanical and Production Engineering
(MPE)

Islamic University of Technology (IUT)

DECLARATION

I hereby declare that this thesis entitled "Design and Analysis of Heat Sink Configurations for Passive Cooling of Solar Panels" is an authentic report of study carried out as requirement for the award of degree B.Sc. (Mechanical Engineering) at Islamic University of Technology, Gazipur, Dhaka, under the supervision of Prof. Dr. Md. Hamidur Rahman, Professor, MPE, IUT in the year 2022.

The matter embodied in this thesis has not been submitted in part or full to any other institute for award of any degree.



Ishtiaq Ahmed

170011048



Hossain Azmain Farhin

170011045



Saziea Afrin Heme

170011007

Acknowledgement

In the Name of Allah, the Most Beneficent, the Most Merciful

The journey through the completion of this thesis required immense effort from every individual involved. The completion of this thesis would have been far from reality if it were not for the constant support from a few dedicated individuals who guided us through the entire study. First and foremost, we would like to express our heartfelt gratitude to Prof. Dr. Md. Hamidur Rahman for being our esteemed supervisor and providing his expert insight for setting our goals clearly, as well as building a strong baseline for our thesis. His insightful instructions helped us to envision the results that we had to aim for from the very beginning of our thesis work. Additionally, we would like to express our deep appreciation to Mr. Md. Azazul Haque from King Fahd University of Petroleum and Minerals (KFUPM) for his invaluable guidance in teaching us the fundamental steps for our work. It would have been impossible to form the research methodologies and seemingly endless iterations of the simulations in this work without his mentorship. Last, but not the least, each of us would like to extend our acknowledgements to our respective parents for being the resilient support during the long, sleepless nights of work on this thesis.

ABSTRACT

The reduction in efficiency of polycrystalline solar panels at very high operating temperatures demands the implementation of effective cooling solutions to dissipate the excess heat from the photovoltaic (PV) module. Passive cooling solutions such as the use of heat sinks provide effective and economical ways to reduce the working temperature of PV modules while making zero contribution to emissions and climate change. The performance of the heat sink is highly dependent on the design geometry and the arrangement of the heat sinks over the lower surface of the solar panel. This study aims to find the performances of five different geometries of aluminium heat sinks to be used for cooling solar panels. Additionally, a comparative analysis of their relative performances under controlled environmental variables is made to find out the best performing model among the selections. The study is performed by numerical simulations under steady-state analysis, where the numerical model is validated using verified, previously published research. The results show that an arrangement of solid T shaped aluminium fins as heat sinks provides the best performance among the five geometries chosen for comparison, while perforated heat sinks perform relatively worse. The best performing geometry provides 3.14% further reduction in PV module temperature compared to its perforated counterpart. Furthermore, the variation of the average PV module temperature has been compared against the incoming solar radiation or heat flux, ambient temperature, as well as the convection heat transfer coefficients in respective graphs for each heat sink geometry, where the relationship between each pair of data has been identified. The analysis reveals that performance differences may be better observed at low values for the convection coefficient and high values for the ambient temperatures. As the methodology followed in this study provides a base model for comparing the relative performances of the heat sink geometries chosen, the same model can be applied to compare other heat sink geometries to establish comparison among themselves as well, thus providing scopes of continuation of this work.

Keywords: Photovoltaic module, solar panel, heat sink, aluminium, passive cooling, steady state analysis.

TABLE OF CONTENTS

ABSTRACT.....	v
TABLE OF CONTENTS	vi
LIST OF FIGURES	viii
LIST OF TABLES	xi
NOMENCLATURE.....	xii
CHAPTER ONE	
INTRODUCTION	
1.1 BACKGROUND OF THE STUDY	1
1.2 RESEARCH PROBLEM STATEMENT	3
1.3 GOALS AND OBJECTIVES.....	3
1.4 SCOPES AND LIMITATIONS	4
1.5 ORGANIZATION OF THE STUDY	4
CHAPTER TWO	
LITERATURE REVIEW	
2.1 SOLAR PANEL CONSTRUCTION AND PV CELL CHARACTERISTICS	7
2.2 PV PERFORMANCE AND COOLING	9
2.3 REVIEW ON PREVIOUS RESEARCH	12
CHAPTER THREE	
RESEARCH DESIGN	
3.1 METHODOLOGY	17
3.2. GOVERNING EQUATIONS.....	18
3.3 HEAT SINK MODELS	20
3.3.1 Solid L Fins.....	20
3.3.2 Perforated L Fins.....	22

3.3.3 Solid T Fins.....	23
3.3.4 Perforated T Fins.....	24
3.3.5 Wire Mesh	25
3.4 3D MODELLING.....	26
3.5 GRID INDEPENDENCE TEST	28
3.6 MODEL VALIDATION.....	34
CHAPTER FOUR	
RESULTS AND DISCUSSION	
4.1 FINAL SIMULATION PARAMETERS	38
4.2 RESULTS, ANALYSIS AND DISCUSSION	38
CHAPTER FIVE	
CONCLUSION AND RECOMMENDATION	
5.1 CONCLUSION.....	57
5.2 RECOMMENDATION AND FUTURE SCOPES	58
REFERENCE.....	59
ADDITIONAL CONTENT	
CD ROM WITH SOFT COPY	

LIST OF FIGURES

Figure 1.1: Cumulative Global Data for Installed Capacity of Solar Photovoltaics.....	2
Figure 1.2: Flow Chart for the Chapters and Respective Contents.	6
Figure 2.1: Components of a Photovoltaic (PV) Unit.	7
Figure 2.2: Monocrystalline (left) and Polycrystalline (right) PV Cell Appearances. .	9
Figure 3.1: Structure and Dimensions of a Solid L Fin.	21
Figure 3.2: Layout of Fin Placement for Solid L Fins.	21
Figure 3.3: Structure and Dimensions of a Perforated L Fin.	22
Figure 3.4: Layout of Fin Placement for Perforated L Fins.	22
Figure 3.5: Structure and Dimensions of a Solid T Fin.	23
Figure 3.6: Layout of Fin Placement for Solid T Fins.	23
Figure 3.7: Structure and Dimensions of a Perforated T Fin.	24
Figure 3.8: Layout of Fin Placement for Perforated T Fins.	24
Figure 3.9: Structure and Dimensions of a Wire Mesh.	25
Figure 3.10: Layout of Placement for Wire Mesh.	25
Figure 3.11: Heat Transfer Modelling for the PV Module.	28
Figure 3.12: Comparison of Mesh for (a) Coarse, (b) Medium, (c) Fine and (d) Superfine Sizes for Solid T Fins.	31
Figure 3.13: Mesh at Fine Element Size for (a) Solid L Fins, (b) Perforated L Fins, (c) Solid T Fins, (d) Perforated T Fins, and (e) Wire Mesh.	32
Figure 3.14: Grid Independence Tests for Solid L Fins, Perforated L Fins, Solid T Fins, Perforated T Fins, and Wire Mesh.	33
Figure 3.15: Recreation of the Experimental Model for Validation.	35
Figure 3.16: Superfine Mesh for Experimental Model with 33799 Elements.	35
Figure 3.17: Graphical Comparison of Experimental [41] and Simulated Results. ...	37
Figure 4.1: Average PV Module Temperature VS Ambient Temperature at Different Convection Coefficients for Solid L Fins.	39
Figure 4.2: Average PV Module Temperature VS Ambient Temperature at Different Convection Coefficients for Perforated L Fins.	40
Figure 4.3: Average PV Module Temperature VS Ambient Temperature at Different Convection Coefficients for Solid T Fins.	41
Figure 4.4: Average PV Module Temperature VS Ambient Temperature at Different	

Convection Coefficients for Perforated T Fins.....	42
Figure 4.5: Average PV Module Temperature VS Ambient Temperature at Different Convection Coefficients for Wire Mesh.....	43
Figure 4.6: Average PV Module Temperature VS Solar Radiation at Fixed Ambient Temperature and Different Convection Coefficients for Solid T Fins.....	46
Figure 4.7: Average PV Module Temperature VS Solar Radiation at Fixed Convection Coefficient and Different Ambient Temperatures for Solid T Fins.....	46
Figure 4.8: Temperature Contour for PV Module only at Ambient Temperature of 30 °C, Heat Flux of 800 W/m ² and Convection Coefficient of 12 W/m ² K for Solid L Fins.....	49
Figure 4.9: Temperature Contour for Solid L Fins at Ambient Temperature of 30 °C, Heat Flux of 800 W/m ² and Convection Coefficient of 12 W/m ² K.....	49
Figure 4.10: Temperature Contour for PV Module only at Ambient Temperature of 30 °C, Heat Flux of 800 W/m ² and Convection Coefficient of 12 W/m ² K for Perforated L Fins.....	50
Figure 4.11: Temperature Contour for Perforated L Fins at Ambient Temperature of 30 °C, Heat Flux of 800 W/m ² and Convection Coefficient of 12 W/m ² K.....	50
Figure 4.12: Temperature Contour for PV Module only at Ambient Temperature of 30 °C, Heat Flux of 800 W/m ² and Convection Coefficient of 12 W/m ² K for Solid T Fins.....	51
Figure 4.13: Temperature Contours for Solid T Fins at Ambient Temperature of 30 °C, Heat Flux of 800 W/m ² and Convection Coefficient of 12 W/m ² K.....	51
Figure 4.14: Temperature Contour for PV Module only at Ambient Temperature of 30 °C, Heat Flux of 800 W/m ² and Convection Coefficient of 12 W/m ² K for Perforated T Fins.....	52
Figure 4.15: Temperature Contour for Perforated T Fins at Ambient Temperature of 30 °C, Heat Flux of 800 W/m ² and Convection Coefficient of 12 W/m ² K.....	52
Figure 4.16: Temperature Contour for PV Module only at Ambient Temperature of 30 °C, Heat Flux of 800 W/m ² and Convection Coefficient of 12 W/m ² K for Wire Mesh.....	53
Figure 4.17: Temperature Contour for Wire Mesh at Ambient Temperature of 30 °C, Heat Flux of 800 W/m ² and Convection Coefficient of 12 W/m ² K.....	53
Figure 4.18: Comparison of All Heat Sink Models at Convection Coefficient of 8 W/m ² K.....	54

Figure 4.19: Comparison of All Heat Sink Models at Convection Coefficient of 12 W/m²K.55

Figure 4.20: Comparison of All Heat Sink Models at Convection Coefficient of 16 W/m²K.55

Figure 4.21: Average PV Module Temperature for all Heat Sink Models at fixed values of Convection Coefficient, Heat Flux and Ambient Temperature.....56

LIST OF TABLES

Table 2.1: Comparison between Active and Passive Cooling Methods for Solar Panels.	11
Table 2.2: Summary of Literature Review.....	15
Table 3.1: Dimensions of Layers in the PV Module.....	18
Table 3.2: Physical and Thermal Properties of Components in the Setup.....	18
Table 3.3: Grid Independence Test Parameters.	30
Table 3.4: Data from Experimental Results [41] and Simulated Results.	36
Table 4.1: Simulation Results for Solid L Fins.....	39
Table 4.2: Simulation Results for Perforated L Fins.	40
Table 4.3: Simulation Results for Solid T Fins.....	41
Table 4.4: Simulation Results for Perforated T fins.	42
Table 4.5: Simulation Results for Wire Mesh.....	43

NOMENCLATURE

PV	Photovoltaic
EVA	Ethyl Vinyl Acetate
PVF	Polyvinyl Fluoride
STC	Standard Test Conditions
AM	Air Mass
q_{cond}	Conduction Heat Transfer Rate
k	Thermal Conductivity
∇T	Temperature Gradient
T	Temperature
q_{conv}	Convection Heat Transfer Rate
h_c	Convection Coefficient
A	Cross Sectional Area
T_s	Surface Temperature
T_{amb}	Ambient Temperature
q_{rad}	Radiation Heat Transfer Rate
ε	Emissivity
σ	Stefan-Boltzmann Constant
FEA	Finite Element Analysis

Subscripts

i	Layer
c	Convection
cond	Conduction
rad	Radiation
s	Surface
g	Glass Cover
E	EVA
P	PV Layer
H	Heat Sink Layer

CHAPTER ONE

INTRODUCTION

1.1 BACKGROUND OF THE STUDY

One of the biggest priorities in the present times is the efficient generation of power from renewable sources of energy. The incoming radiation from the Sun is one of the most abundant forms of energy that is available to be utilized as a source of renewable energy. Solar energy can be harnessed and converted into electricity through solar panels. These panels are devices that incorporate semi conductive photovoltaic (PV) cells which allow the direct conversion of a small quantity of incoming solar radiation, or heat flux, into electrical energy. This process is carbon neutral and does not produce any greenhouse gases, so it does not contribute to climate change. The implementation of solar panels has been widespread, starting from small scale grid installations in households to large scale field layouts that provide a substantial amount of electricity to the national grid, such as the 10 MW solar power plant in Ramagundam, India [1]. Installation capacity for electricity generation through solar PV has evolved rapidly over the last few years, with a global total installed capacity of 843,086 MW solely from solar PV by 2021, as reported by the International Renewable Energy Agency [2]. **Figure 1.1** shows the growth of total installed capacity of solar PV from 2011 to 2021.

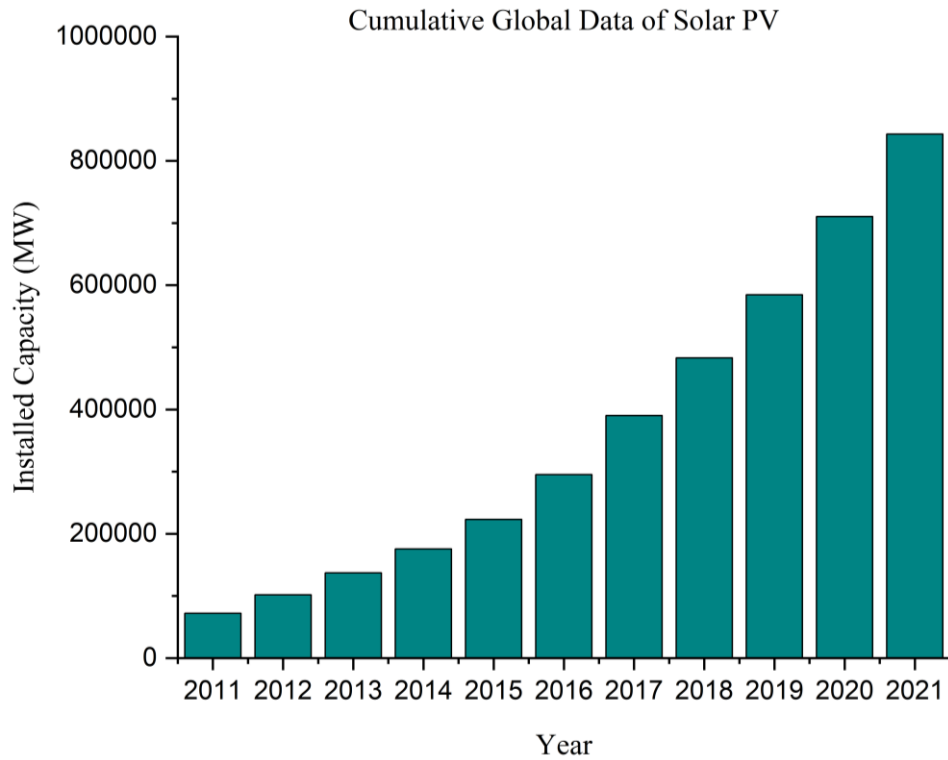


Figure 1.1: Cumulative Global Data for Installed Capacity of Solar Photovoltaics.

In spite of having the appeal to producing clean energy, solar panels lack a high degree of efficiency in energy conversion, as a significant portion of the heat flux remains in the form of thermal energy. With a small quantity of incoming solar radiation converted to electricity, the residual heat combined with the waste heat from the conversion add up to the high temperature of the PV modules. Excessive temperature build up leads to overheating of the PV modules, which leads to a sharp drop in the voltage output of the PV module, resulting in a much lower electrical output and overall efficiency [3]. To counteract this negative effect, novel cooling approaches for reducing the operating temperatures of PV modules have been suggested over the years, with various active and passive cooling methods suggested to help improve the efficiency of solar panels [4]. Passive methods, especially using highly conductive heat sinks, have shown great potential to be effective as cooling solutions for solar panels, primarily due to their ease of implementation and low costs. The effectiveness of such components vary largely on their design factors and dependencies on operational conditions, which requires dedicated work to be carried out to prove their feasibility. This study has been carried out with the aim of comparing five types of aluminum heat sink designs and their corresponding configurations that can be installed in solar panels to reduce the

temperatures of the PV modules. A simple numerical model is validated by comparing with previous experimental data, and then used to analyze the performance of each variation of design in terms of temperature reduction of the solar panels. The simulations are carried out in ANSYS Steady State Thermal software, and the results are presented in forms of tables, graphs and temperature contours. These are analyzed to compare the performance of the heat sink configurations relative to one another.

1.2 RESEARCH PROBLEM STATEMENT

Photovoltaic (PV) modules in solar panels operate at reduced efficiency when exposed to high temperatures from incoming solar radiation, producing lower quantity of electricity from the heat flux as well as reducing the life expectancy of the solar panel. Installing heat sinks allows passive cooling of solar panels, which reduces the operating temperature of the PV module. The challenge lies in finding the effectiveness of various designs on heat sinks, and in comparing their effectiveness in contrast to one another under specified conditions. Therefore, the performance of PV modules combined with heat sinks needs to be evaluated under controlled parameters without the randomization of environmental variables. Under identical conditions, the PV module temperature results from using various heat sink designs need to be evaluated using a set of values for incoming solar radiation and ambient temperatures.

1.3 GOALS AND OBJECTIVES

The primary goal of this study is to compare the relative performances of five heat sink designs for passively cooling solar panels. Additionally, the performances of these heat sinks are to be presented in a comprehensive manner as well to determine help visualize their effectiveness. The objectives are outlined as follows:

- To pick 5 geometrically different aluminum heat sink designs for cooling solar panels.
- To find experimental data from prior research and use it for validating planned numerical model.
- To set up the simulations as per specified operating conditions and standard properties of the materials used.

- To find the temperature values of solar panel at the end of simulation for each design by varying the convective heat transfer coefficient and ambient temperature.
- To provide temperature contours for each heat sink model to help visualize the temperature profile on the PV module under the tested conditions.
- To plot detailed, comparative graphs of PV module temperature against ambient temperature for each variation.
- To compare the reduction of PV module temperature for each model and determine the best design based on simulation results and feasibility.

1.4 SCOPES AND LIMITATIONS

This study covers the procedure for evaluation and analysis of heat exchange between solar panels and heat sinks in the computational domain, while keeping all of the important physical considerations and boundary conditions under control as required. The selection of heat sink material, particular geometries, and controllable variables under which the solar panel is expected to operate have been addressed. The outcome of this study is aimed at better understanding the effectiveness of the heat sink designs for solar panels, and thus figuring out scopes of further improvement or additional research. The primary limitation for this study has been the hardware limitations for performing the most precise simulations; grid sensitivity tests have been used to obtain acceptable meshing levels for the materials in the simulation software to produce reliable results. Additionally, the aftermath of the recent COVID-19 pandemic has left little scope for fabricating the heat sinks for performing hands-on experiments, therefore older experimental data under identical conditions has been used to validating the simulation results.

1.5 ORGANIZATION OF THE STUDY

In the upcoming chapters, the study is presented in a sequenced order.

A literature review is presented, with the first part providing background information on solar panels, PV panel characteristics and cooling methods, all collected from various publications and textbooks. The second part contains summarization of previous research work on passive cooling of solar panels, mostly from publications in

reputed journals. This chapter is intended to provide a clear idea of the addressed topic, what has been done before, and how it provides scope for this study to contribute to the work.

The research methodology is presented in detail, along with the configurations for heat sinks to be tested. Governing equations, modelling considerations, grid independence test and validation of simulated results with previous experimental data are added afterwards.

Chapter 4 presents the detailed results and analysis using numerical and graphical data. Comparison is made among the proposed geometries and their cooling effectiveness is analyzed from the obtained results.

The final chapter concludes the analysis of the results and notes possible scopes for improving or expanding upon this study, in terms of direct modification, or further research.

A simple flow chart representing the chapter arrangement is shown in **Figure 1.2**.

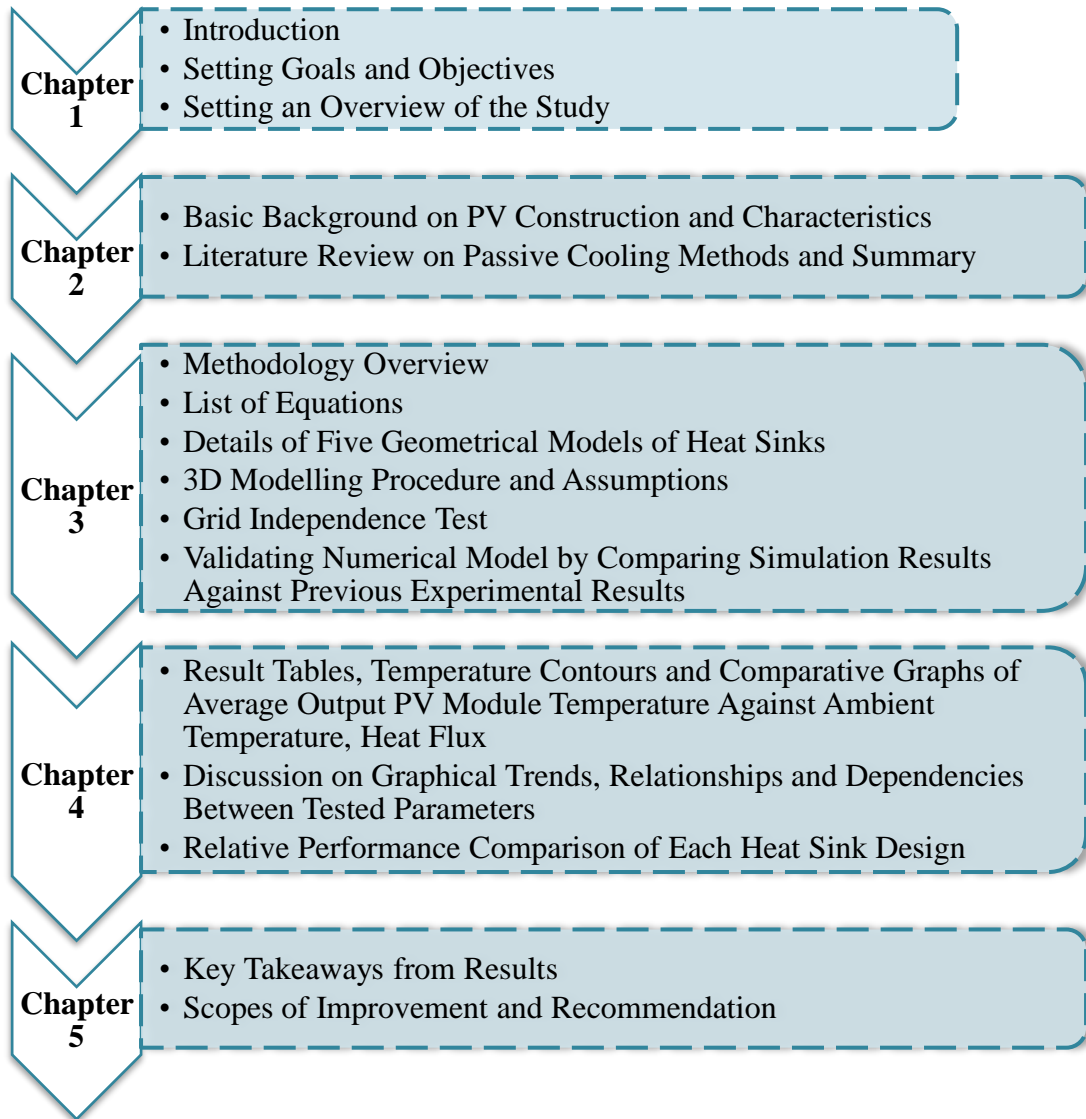


Figure 1.2: Flow Chart for the Chapters and Respective Contents.

CHAPTER TWO

LITERATURE REVIEW

2.1 SOLAR PANEL CONSTRUCTION AND PV CELL CHARACTERISTICS

The components of a basic solar panel unit is illustrated in **Figure 2.1** to better understand its constructional features by the arrangement of layers in the main PV unit.

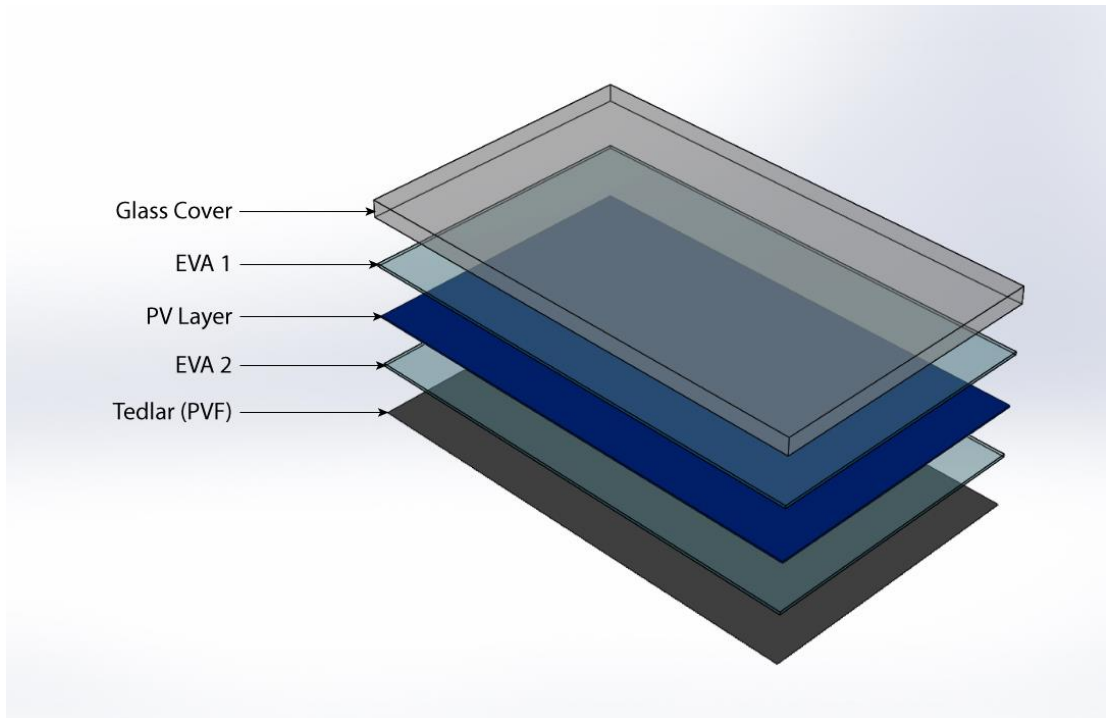


Figure 2.1: Components of a Photovoltaic (PV) Unit.

A glass cover encapsulates the top portion of the solar panel, and acts as the primary surface through which incoming solar radiation enters the panel. It serves two main purposes, one being entrapment of the sunlight that enters, and the other being a protective material against environmental hazards for solar panel such as heavy dust, rain and humidity. Glass is also referred to as glazing material, as it ensures maximum solar radiation transmission to the PV modules by allowing mostly short-wave radiations while blocking the long-wave radiations [5]. The thickness of the glass panel can have a noticeable effect on the PV module performance, as it has been shown that 4 mm of glass panel thickness has higher solar intensity absorption compared to other similar thicknesses [6].

Ethyl Vinyl Acetate (EVA) is a very thin, durable copolymer film of ethylene and vinyl acetate [7]. It has great optical transparency which makes it suitable for being used as encapsulation material for PV modules. However, EVA is prone to degradation from ultraviolet radiation which can change its color, therefore negatively affecting its transparency [8]. Therefore, having a glass cover prevents such issues from arising too early in the lifetime of a solar panel. As shown in **Figure 2.1**, EVA forms the second and fourth layers of the solar panel unit.

Polyvinyl Fluoride (PVF), also known as tedlar, may be defined as a thermoplastic polymer consisting of a repeating unit made from carbon, hydrogen and vinyl fluoride [9]. PVF has been extremely popular for use as a protective material for solar applications, especially solar panels. PVF possesses very desirable chemical, electrical and mechanical properties, some of which are particularly useful for solar panels. It has high resistance to corrosion and degradation from exposure to sunlight and ultraviolet rays, very low chemical reactivity, as well as high thermal stability, making it an essential material which is used as the backing layer of solar panels [10].

The main constituent of a solar panel is an arrangement of PV cells forming a PV layer, which is responsible for the energy conversion. PV cells are able to convert incoming solar radiation directly to electricity. The light from incoming solar radiation creates an electric field between the PV cells, producing an output voltage and current [11]. PV layers are usually manufactured as either films or in crystalline forms, the latter of which further classifies into monocrystalline and polycrystalline structures. Monocrystalline silicon is made from a single silicon crystal, so a monocrystalline module has an ordered pattern of arrangement [12]. Its appearance is a spotless and black texture. In contrast, polycrystalline silicon has a blue hue, and it is made from multiple silicon crystals that are melted as a whole. The visual differences are both in the color as well as in the pattern of the grid of the panel, as shown in **Figure 2.2** [13].

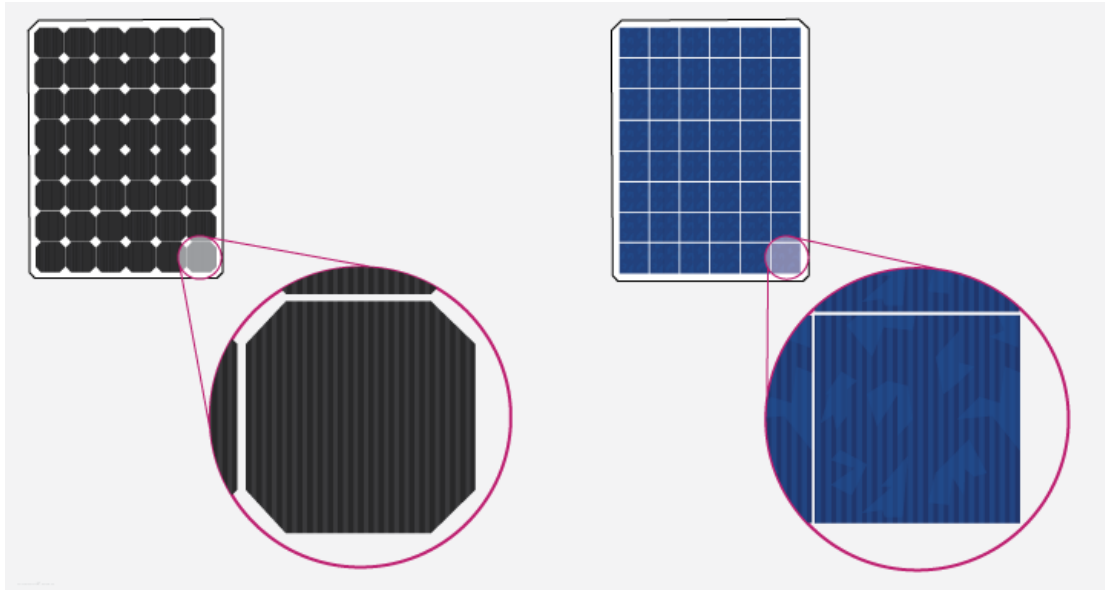


Figure 2.2: Monocrystalline (left) and Polycrystalline (right) PV Cell Appearances.

2.2 PV PERFORMANCE AND COOLING

Typically, solar panels are initially tested for their performance thresholds in controlled environments under standard test conditions (STC), where the PV module temperature is 25 °C, irradiance is 1000 W/m², and air mass (AM) is 1.5 [14]. Such tests imply favorable numbers for PV cell efficiency, such as single-junction silicon cells showing efficiencies ranging around the 27% mark [15]. However, in real-life scenarios, the performance of solar panels may vary to a large extent, mainly due to a combination of both controllable and uncontrollable factors involved in the heat transfer and energy conversion of PV cells. In that case, the conversion process of PV cells has a reduced efficiency, as regular polycrystalline PV cells can only convert about 15% of irradiation into electrical energy, while some organic PV cells can achieve up to 17% efficiency [16]. Apart from materialistic limitations in direct conversion capabilities of the PV cells themselves, the conversion of solar radiation into heat can have a significantly detrimental impact on their efficiency. Depending primarily on the amount of solar radiation and the ambient air temperature, an almost linear decrease in PV cell efficiency is observed with increase in PV cell temperature [17]. A previous work has shown that an increase in temperature of crystalline silicon cells by 1 °C results in a reduction of their efficiency by about 0.45% [18]. Prolonged exposure to high levels of temperature can severely undermine the power output of PV cells by as much as 3.19%

per year under hot, tropical climate with high levels of humidity [19]. The elevated levels of temperature also affects the material composition of PV modules. Obtaining uniform temperature distribution throughout the surface area of the panel is a difficult task to accomplish because the degradation over time alters the material condition. In the event that the temperature distribution is non-uniform, the PV cell temperature and the series resistance in the layers increases, resulting in a reduced electrical output, hence lower conversion efficiency [20]. The life expectancy of electrical equipment can be shortened over time due to the fluctuation of temperature especially in the metallic and semi-metallic parts. Electrical equipment is prone to degradation from thermal cycles that expand and contract the internal materials and their layers on heating and cooling, respectively [21]. Studies have shown this degradation to be significant in reducing the performance and efficiency of solar panels [22]. The operation of solar panels requires direct exposure to sunlight which has varying levels of intensity over the course of daytime. This leads to continuously changing temperatures of the PV modules, affecting their output as well as life expectancy in the long run. With both of these factors being key to analyzing the economic feasibility of solar panels, solutions are required for improving the reliability and durability of solar panels [23]. In order to reduce the aforementioned negative effects, the heat from the PV modules must be dissipated or transferred to some other medium, so that the operating temperature of PV modules drop, and ultimately efficient conversion to electricity is achieved. Therefore, effective cooling solutions for solar panels need to be improvised.

The methods of cooling solar panels may be categorized into either active or passive cooling techniques. Active cooling employs moving a coolant fluid over the solar panel by using an externally powered source such as a pump or a fan, while passive cooling eliminates the need of external power and relies on components like heat sinks or heat pipes to dissipate the heat by basic methods of heat transfer: conduction, convection and radiation [24]. A brief look at the key differences between active and passive cooling methods can be found in **Table 2.1**.

Table 2.1: Comparison between Active and Passive Cooling Methods for Solar Panels.

Active Cooling	Passive Cooling
Needs power source Uses forced convection Power usage incurs operational cost Expensive to set up Complicated design Needs frequent maintenance Higher cooling potential Cooling rate can be increased on demand	Uses zero power Uses natural convection Zero operational cost Relatively cheaper installation cost Easy to design Needs very little maintenance Lower cooling potential Cooling rate is fixed for material used

The main attractions of passive cooling methods are the advantages of needing zero power input and being economical due to zero operational costs, therefore these methods are considered to be best in improving the practical efficiency of the solar panels overall [25]. Plenty of passive cooling techniques exist for the purpose, each with varying positive and negative aspects of its own. One of the most straightforward methods of passive cooling for solar cells is the use of heat sinks made from materials with high thermal conductivity. A heat sink is a block of material with good conductivity designed to act as a heat exchanger, typically between a hot solid surface and a working fluid. In case of passive cooling of solar panels, a heat sink is attached to the tedlar, usually by a thermal compound adhesive. Heat from the PV module is transferred to the tedlar, and then the heat sink absorbs that heat and ejects it to the surrounding air mostly by conduction and convection. Natural convection facilitates the heat transfer from the hot outer surfaces of a heat sink to the relatively colder ambient air. Metals with high thermal conductivity such as copper and aluminium are great choices as heat sink materials. Other factors such as availability, cost, weight, as well as resistance to thermal cycling are important considerations for choosing a heat sink material. When considering thermal properties exclusively, copper is superior to aluminium due to having almost twice as much thermal conductivity. However, copper has a density almost three times greater than that of aluminium. This makes a heat sink made from copper significantly heavier. As a result, copper becomes a worse choice overall when compared to aluminium. Furthermore, the high density amounts to a greater cost as a greater mass of material needs to be purchased for a specified volume

of heat sink. Therefore, aluminium is the most common choice for heat sink material due to its low mass, wide availability, and ultimately low cost.

2.3 REVIEW ON PREVIOUS RESEARCH

Over the years, plenty of studies have been carried out through numerical analysis and experiments to analyze and find out suitable designs and applications of metal heat sinks on solar panels in order to reduce their average operating temperatures, thus improving their electrical efficiencies. The main idea would be to use passive cooling through natural convection through different designs of heat sinks. This section discusses the work done on the various types of heat sink designs. The information has been sourced from well-reputed journals like Elsevier and Springer.

Solid fins have been shown as an effective design for heat sink to be used in solar panels. One of the most basic experiments to see whether the output of a solar panel changed by addition of heat sink was performed by Gotmare et al. [26]. In the experiment, two 37 W solar panels were used under a solar irradiance of 1000 W/m², one with an aluminium heat sink, and the other without. The heat sink consisted of long, straight aluminium fins that ran from one side to the opposite, thus covering the entire width of the solar panel. Using the heat sink resulted in a decrease of the PV module temperature by about 2.5 °C in average compared to that in the bare panel, which amounts to a 4.2% drop in PV module temperature. El Mays et al. [27] showed through experiment that using finned aluminium heat sinks drastically reduced the operating temperatures of solar panels, therefore improving electrical efficiency. In the experiment, a 30 W solar panel was cooled using a large finned aluminium heat sink with dimensions of 60 cm, 28 cm, and 4 cm by length, width, and thickness, respectively. The outcome of the experiment resulted in an average temperature drop of 6 °C from the average temperature of the standard panel without heat sink. Consequently, this led to an increase in efficiency of the panel by 1.77%. The study also revealed that the efficiency of the PV module was in fact inversely proportional to the solar irradiation, that is, higher irradiation resulted in overheating of the PV module. Bayrak et al. [28] used 10 geometries of aluminium heat sinks with fins of different lengths and arrays on a 75 W polycrystalline panel of 770 mm, 670 mm, and 25 mm by length, width, and thickness, respectively. For any of the heat sink geometries, the temperature drop of the PV module was anywhere from 3 °C to 6 °C. It was concluded

that a heat sink of size 7 cm, length 20 cm with 26 aluminium fins of total length 520 cm in a staggered-horizontal array would provide the highest energy and exergy efficiencies of 11.55% and 10.91%, respectively. The increase in energy efficiency was 2.82%. A parametric study by Elbreki et al. [29] was based on lapping aluminium fins and their effectiveness as heat sink for two STF-040P1 PV modules. Without any cooling, the panels reached operating temperature of up to 64.3 °C under irradiation of 1000 W/m² and an electrical efficiency of 9.81%. Adding the heat sink with lapping aluminium fins of up to 2 mm thickness drastically reduced the maximum temperature by 24.57 °C, and the electrical efficiency increased to 11.2%. Although this design looks promising, the fin shape is comparatively difficult to manufacture and adhere to a solar panel compared to the commonly used fins.

An innovative approach to modifying the fin design was to create perforations through fins on the heat sink. Arifin et al. [30] carried out experiments and simulations on 50 W solar panels to find their temperatures and electrical efficiencies when using aluminium heat sink with perforated fins, and without any heat sink at all. The numerical study showed that at ambient temperature of 35 °C under a heat flux of 1000 W/m², the average temperature of the PV panel with heat sink turned out to be 72.8 °C, which was 12.5 °C lower than that of the PV panel without heat sink. From the experiments, an increase of 2.6% in electrical efficiency was observed, with an average temperature reduction of up to 10 °C in PV panel temperature. The cooling effectiveness of perforated ribs on metal heat sinks was numerically studied by Popovici et al. [31] by making changes to the angle and height of the ribs with the base plate of the heat sink. The results showed that using the fins reduced the PV module temperatures by a noticeable margin, with a decrease of 10 °C in PV module temperature when using the smallest ribs. However, the study used a low heat transfer coefficient of 8 W/m²K and low solar radiation of 500 W/m², so the effectiveness of the ribs at higher levels of irradiation was yet to be seen. One of the most recent analytical works on passive cooling solutions for PV panels was by Haque et al. [32] where 3 different types of aluminium heat sinks in a total of 19 arrangements were analyzed to find their effectiveness. At 35 °C ambient temperature, solar radiation of 800 W/m², and convective heat transfer coefficient of 10 W/m²K, a combined heat sink type made of a flat base and fins with small holes produced the best results where the temperature of

the PV panel was reduced to 56.23 °C in contrast to a base panel reaching 73.84 °C under the same conditions.

Through simulations carried out in ANSYS Fluent, Salami et al. [33] demonstrated the effects of using four different shapes of fins with different spacing among them to passively cool down PV cells. Fins of rectangular, trapezoidal, curved, and pin shapes were used, and the duct heights were 4 cm, 6 cm, 8 cm, and 10 cm. Additionally, the work involved variation of incoming wind velocity on the fins. Results indicated that the best possible outcome could be achieved using rectangular fins with duct height of 4 cm under velocity magnitude of 3 m/s, allowing a maximum temperature of 33 °C for the PV cells. Marinić-Kragić et al. [34] improvised a design where two slits are made on the PV module itself to facilitate the dissipation of heat. A 50W PV module was experimentally tested under the Mediterranean climate. The best orientation turned out to be the PV panel having two slits of 300 mm length and 10 mm width, perpendicular to the axis of tilt of the PV panel, which ended up with an average reduction in PV panel temperature by 3 °C, as long as the wind speed stayed below 5 m/s. An extensive experiment was conducted by Selimefendigil et al. [35] using porous aluminium metal foam fins of thicknesses of 6 mm and 10 mm to analyze their effects on 75 W polycrystalline solar panels. The analysis showed that the thicker, porous 10 mm fins produced the greatest output power, with the maximum power difference being 7.26 Watts. In terms of surface temperature, the difference between a non-fin panel and a panel with 10 mm thick porous fins was 1 °C. Another experiment involving open-cell copper metal foam fins as heat sink for PV panels to enhance their performance was carried out by Hasan et al. [36]. The 50 W PV panels were fitted with different arrangements of porous copper fins, with numbers evenly ranging from 4 to 10 and distances between them varying for each arrangement. Upon investigation, using 10 fins reduced the average temperature of the PV panel by 3.8 °C, while the average power output was 4.9% higher. Kim et al. [37] performed experiments and numerical study on the cooling effectiveness of iron and aluminium in the form of a wire mesh. In the experiment, a very large PV module was used with a peak rating of 340W. At irradiance of 800 W/m², the reduction in PV cell temperature was 1.49 °C and 3.18 °C for iron and aluminium mesh, respectively.

The literature review has been summarized in **Table 2.2**.

Table 2.2: Summary of Literature Review.

Researchers	Material	Heat Sink Design	Panel Rating and/or Dimensions	Solar Radiation	Temperature Drop
Gotmare et al.	Aluminium	Long, solid fin	37 W	1000 W/m ²	2.5 °C
El Mays et al.	Aluminium	Long, solid fin	30 W, 600x280x40 mm	800 W/m ²	6 °C
Bayrak et al.	Aluminium	Varying lengths, solid fins	75 W, 770x670x25 mm	1088 W/m ²	3 °C - 6 °C
Elbreki et al.	Aluminium	Long, lapping solid fins	40 W, 670x530 mm	1000 W/m ²	24.57 °C
Arifin et al.	Aluminium	Small, perforated fins	50 W, 655x670x25 mm	1000 W/m ²	10 °C
Popovici et al.	Aluminium	Long, perforated fins at angles	500x500 mm	500 W/m ²	10 °C
Haque et al.	Aluminium	Flat plate, perforated fins	770x670 mm	800 W/m ²	17.61 °C
Salami et al.	Aluminium	Rectangular, trapezoidal, curved and pin fins	-	900 W/m ²	18 °C
Marinić-Kragić et al.	-	Direct slit in PV module	50 W, 550x650 mm	600 W/m ²	3 °C
Selimefendigil et al.	Aluminium	Porous foam fins	75 W	906 W/m ²	1 °C
Hasan et al.	Copper	Porous foam fins	50 W	770 W/m ²	3.8 °C
Kim et al.	Iron, Aluminium	Wire mesh	340 W	800 W/m ²	1.49 °C, 3.18 °C

The literature review provided above demonstrates numerous designs and applications for heat sinks in PV panels and the respective results from simulations, real life experiments, or a combination of both. The consensus is that there is a decrease in average operating temperature, and hence an increase in electric efficiency of solar panels with heat sink can be observed in contrast to those without. Aluminium is the most preferred choice of material for constructing the heat sinks. The irradiance values vary depending on environmental conditions, or are fixed at a certain value in simulations. However, the design parameters for the heat sinks may vary greatly. The experimental research are all performed under dynamic environmental conditions. Different researchers have used solar panels with different peak power ratings and dimensions. Additionally, very few researchers attempted to compare different types of heat sink geometries under constant conditions. This calls for extensive trials to test the varieties of heat sinks that may be put into use. While one generic shape can be varied in dimensions to compare their effectiveness, there needs to be more work done to compare various types of geometries in similar dimensions for one specific size of solar panel, so that the relative differences in cooling effectiveness of the heat sink geometries can be better understood. Most of the previous research works have used small sized solar panels, so the temperature differences are rather small within their working limits. The base performances of heat sink designs under controlled conditions can also be analyzed by numerical simulation. As difficulties in material acquisition, the time-consuming nature of prolonged tests and financial drawbacks stand as roadblocks in performing hands-on experiments, the role of numerical analysis is significant in continuing the studies for designing and comparing proper heat sink designs. Testing the models on simulation software like ANSYS Thermal can allow continuation of these studies while reducing or eliminating the aforementioned barriers.

CHAPTER THREE

RESEARCH DESIGN

3.1 METHODOLOGY

In this study, five different geometries of aluminium heat sinks are chosen to be used for passively cooling a large solar panel. The test model is divided into two parts, where the first part consists of the main solar panel components, referred to as the PV module, and the other part is the heat sink only. The performances of these heat sinks are evaluated in terms of the amount of relative reduction in PV module temperature, both by magnitude and by percentage difference. For collecting the final data, the minimum, maximum and the average values of PV module temperature have been obtained under various incoming solar radiation or heat flux values and convection coefficients of heat transfer. The average temperatures of the PV module are compared with the ambient temperature to determine the cooling performance of the heat sinks. The performance analysis of the heat sink geometries is to be carried out under steady-state conditions.

As mentioned before, the complete setup for each simulation consists of a PV module and a heat sink. The dimensions of the PV module are 1640 mm in length and 990 mm in width with a maximum peak output of 260 W [38], and the reference temperature is taken as 25 °C. There are five layers of material in the PV module; starting from top, there is a glass cover, followed by a layer of EVA, PV layer, a second layer of EVA, and lastly a tedlar. The dimensions of each layer are given in **Table 3.1**, while the physical and thermal properties of each layer are given in **Table 3.2**. Each designed heat sink is attached to the tedlar by the help of Devcon R2-42. It is a steel-filled, liquid epoxy which acts as a thermal compound as well as adhesive for high temperature working conditions [39]. Aluminium 1100 is used as the heat sink material. Properties for the adhesive and heat sink material are also added in **Table 3.2**.

Table 3.1: Dimensions of Layers in the PV Module.

Layer	Length (mm)	Width (mm)	Thickness (mm)
Glass Cover	1640	990	3
EVA	1640	990	0.5
PV Layer	1640	990	0.3
Tedlar	1640	990	0.1

Table 3.2: Physical and Thermal Properties of Components in the Setup.

Component	Density (kg/m ³)	Thermal Conductivity (W/m.K)	Specific Heat (J/kg.K)
Glass Cover	3000	1.8	500
EVA	960	0.35	2090
PV Layer	2330	148	677
Tedlar	1200	0.2	1250
Adhesive [39]	2118.6	0.58158	1100
Aluminium [40]	2710	222	904

3.2. GOVERNING EQUATIONS

All layers in the solar panel are considered to be solid, homogenous layers. Therefore, the method of heat transfer among these layers is considered to be conduction. The thermal gradients among the layers of material within the solar panel and its ambient environment lead to heat loss by conduction as well. The loss is found from Fourier's Law of Conduction, which is expressed as:

$$q_{cond} = -k \nabla T \quad (1)$$

Here, q_{cond} is the heat transfer rate by conduction, k is the thermal conductivity of the material, and ∇T is the temperature gradient. For three dimensional consideration, the conduction equation for steady-state heat transfer in Cartesian coordinate system is expressed as in Equation (2):

$$\nabla \cdot (K_i \nabla T_i) + \sum Q_i = 0 \quad (2)$$

Here, K_i is the layer thermal conductivity, T_i is the layer temperature, and $\sum Q_i$ represents the summation of other energies in the layer. Since there is no source of heat generation among the layers, and the materials are considered to be isotropic, Equation (2) can be reduced to Equation (3) as:

$$\nabla \cdot (\nabla T_i) = 0$$

Or

$$\frac{\partial^2 T_i}{\partial x^2} + \frac{\partial^2 T_i}{\partial y^2} + \frac{\partial^2 T_i}{\partial z^2} = 0 \quad (3)$$

The majority of heat transfer will be from the surface of the heat sink to the surrounding air through natural convection. The amount of heat dissipated to the surrounding air can be found by the equation from Newton's Law of Cooling, which is expressed as:

$$q_{conv} = h_c A (T_s - T_{amb}) \quad (4)$$

Here, q_{conv} is the rate of heat transfer by convection, h_c is the convection coefficient of heat transfer, A is the cross sectional area or surface area through which the heat is transferred, T_s is the temperature of the surface of the hot object, and T_{amb} is the ambient temperature.

The glass cover at the top of the PV module has high emissivity, so the radiation heat transfer needs to be accounted for. Contrary to this, the aluminium heat sink has very little emissivity. The Stefan-Boltzmann equation can be used to express heat transfer by radiation as:

$$q_{rad} = \varepsilon \sigma A (T_s^4 - T_{amb}^4) \quad (5)$$

Here, q_{rad} is the rate of heat transfer by radiation, ε is the emissivity, σ is the Stefan-Boltzmann constant, A is the surface area through which the heat is transferred, T_s is the hot surface temperature, and T_{amb} is the ambient temperature.

Using these equations, the energy balance in terms of temperature for each layer within the PV module can be expressed by Equations 6 to 11.

Glass cover layer:

$$q_{COND_g} + q_{COND_{g-E}} + q_{CONV_{g-a}} + q_{RAD_{g-a}} - q_g = 0 \quad (6)$$

First EVA layer:

$$q_{COND_E} + q_{COND_{E-C}} + q_{COND_{E-g}} - q_E = 0 \quad (7)$$

PV layer:

$$q_{COND_P} + q_{COND_{P-E}} + q_{COND_{P-H}} - q_P = 0 \quad (8)$$

Second EVA layer:

$$q_{COND_E} + q_{COND_{E-C}} + q_{COND_{E-P}} - q_E = 0 \quad (9)$$

Tedlar layer:

$$q_{COND_P} + q_{COND_{P-E}} + q_{COND_{P-H}} - q_P = 0 \quad (10)$$

Heat Sink layer:

$$q_{COND_H} + q_{COND_{H-P}} + q_{CONV_{H-a}} + q_{RAD_{H-a}} - q_H = 0 \quad (11)$$

3.3 HEAT SINK MODELS

3.3.1 Solid L Fins

Aluminium fins in the shape of “L” are attached to the tedlar by the help of adhesive material. The structure of an individual fin is shown in **Figure 3.1**. The short length side of the fin is in contact with the tedlar, and the long side acts as the part exposed to the surrounding air to dissipate the heat from the tedlar. A total of sixty fins are placed at uniform distances in a grid-like pattern centered on the tedlar. The fin placement is planned according to the layout shown in **Figure 3.2**.

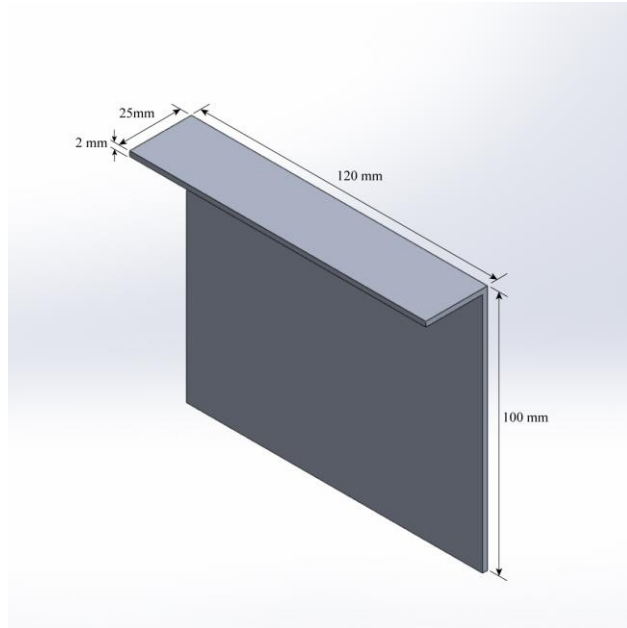


Figure 3.1: Structure and Dimensions of a Solid L Fin.

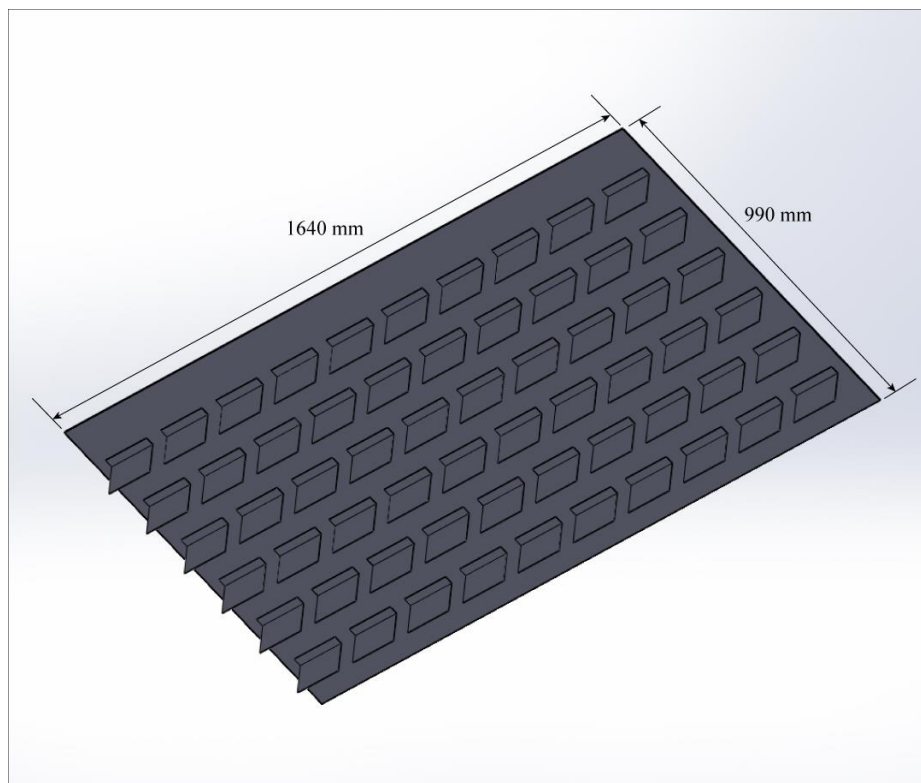


Figure 3.2: Layout of Fin Placement for Solid L Fins.

3.3.2 Perforated L Fins

The “L” shaped fins are now perforated through their large, flat face as shown in **Figure 3.3**. The dimensions of the main fin are maintained same as that of the solid counterpart, and the orientation of adhesion is also kept unchanged. **Figure 3.4** shows the distribution of these fins over the tedlar.

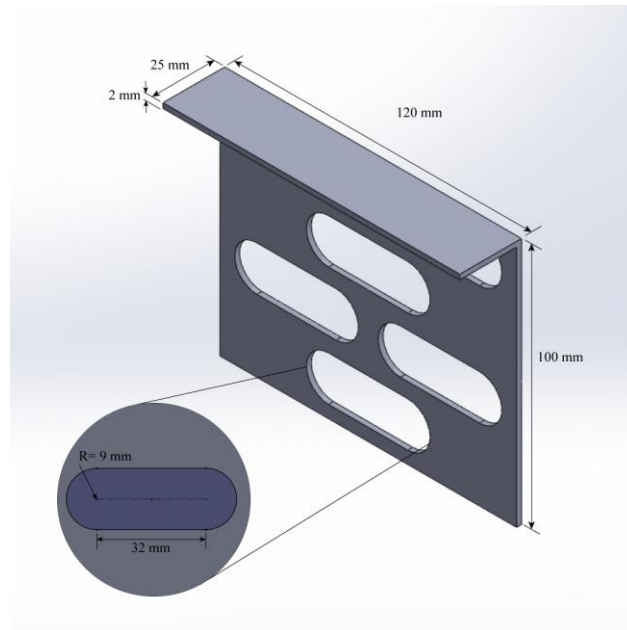


Figure 3.3: Structure and Dimensions of a Perforated L Fin.

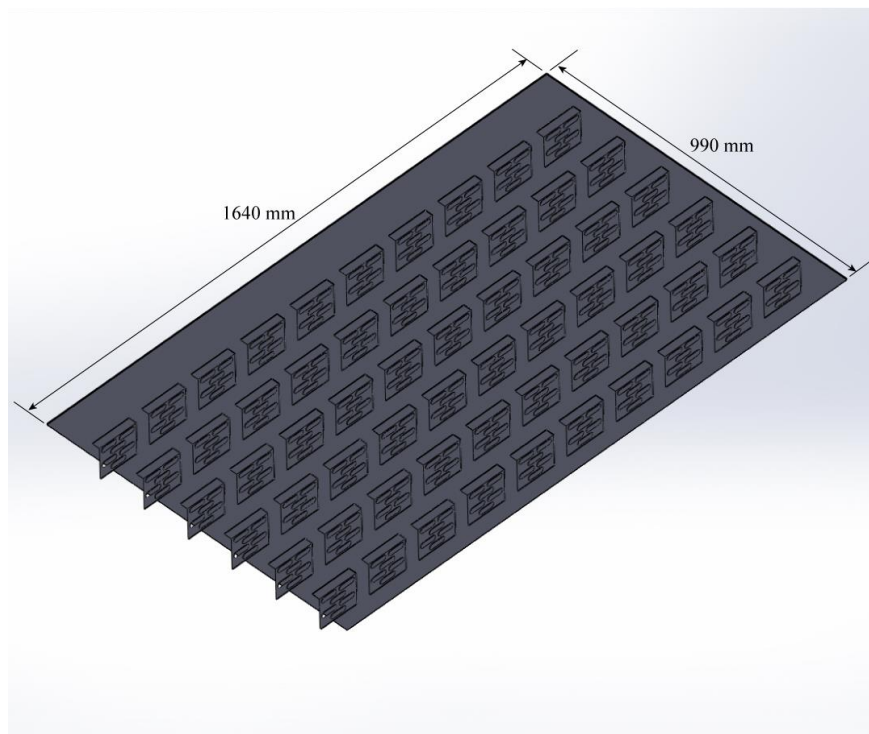


Figure 3.4: Layout of Fin Placement for Perforated L Fins.

3.3.3 Solid T Fins

This geometry is almost identical as the first, except for the fins in this case being in the shape of “T”. **Figure 3.5** depicts the appearance of a solid T shaped fin. Here, the top side of the fin is attached to the tedlar, and the rest is exposed to the surrounding air. In a similar grid-like arrangement, there are sixty fins distributed over the tedlar surface. The distribution is shown in **Figure 3.6**.

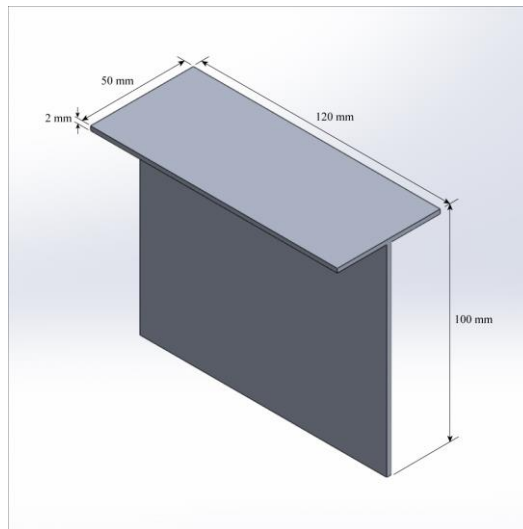


Figure 3.5: Structure and Dimensions of a Solid T Fin.

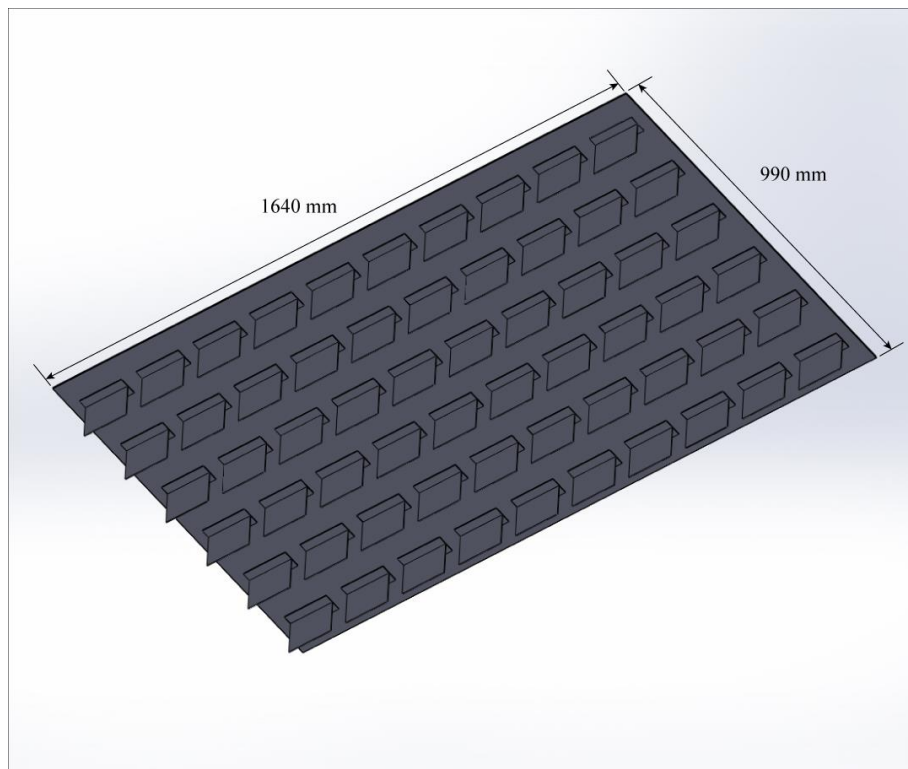


Figure 3.6: Layout of Fin Placement for Solid T Fins.

3.3.4 Perforated T Fins

In a similar manner to the case of L shaped perforated fins, a geometry of T shaped perforated fins are designed with the same perforation dimensions, shown in **Figure 3.7**. The outline of arrangement of the fins is shown in **Figure 3.8**.

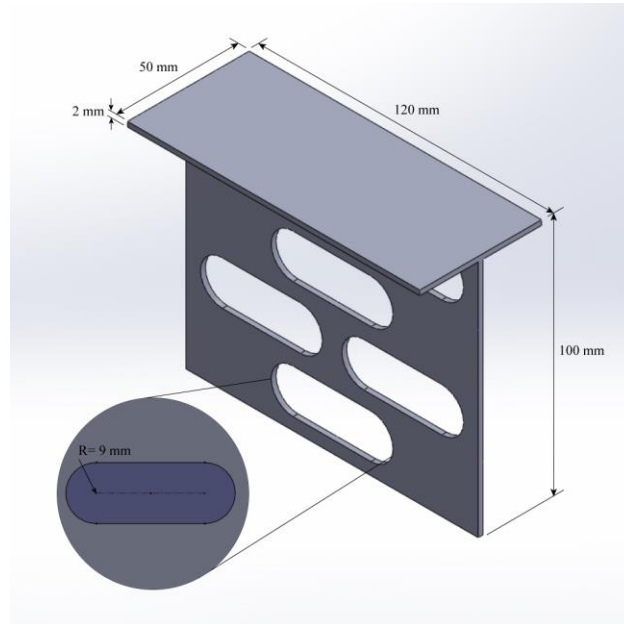


Figure 3.7: Structure and Dimensions of a Perforated T Fin.

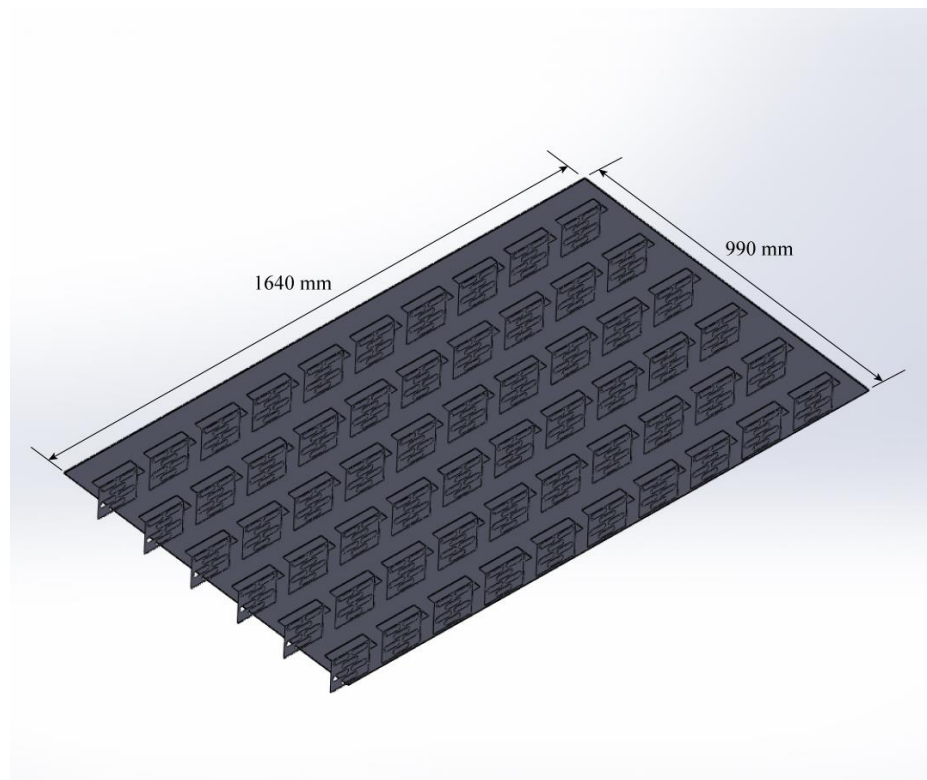


Figure 3.8: Layout of Fin Placement for Perforated T Fins.

3.3.5 Wire Mesh

For this final geometry, a metallic structure in diamond-like shapes made from aluminium in the form of a mesh is to be used for cooling the PV module. A section of the mesh is as depicted in **Figure 3.9**. One side of the mesh will be adhered to the tedlar, and the other side will be exposed to the ambient air. The combination of wire mesh with the PV module is shown in **Figure 3.10**.

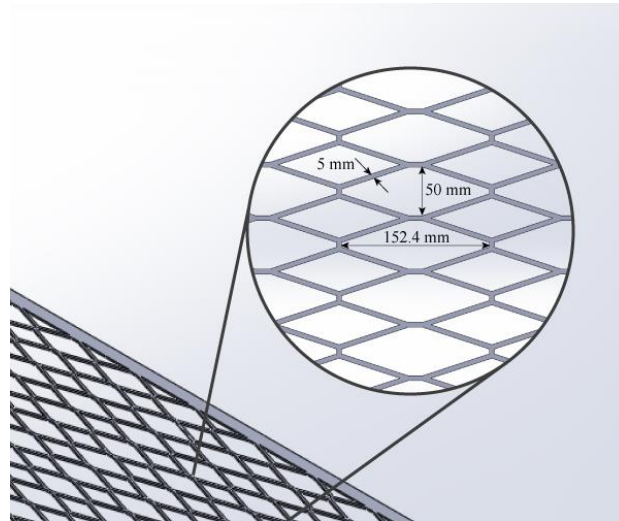


Figure 3.9: Structure and Dimensions of a Wire Mesh.

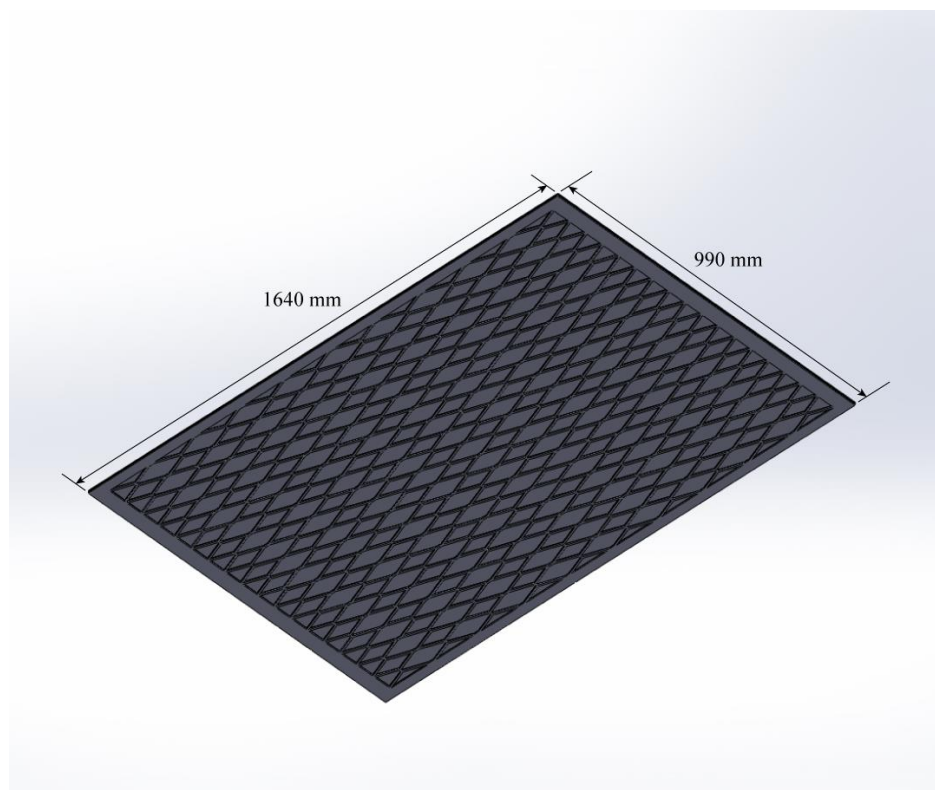


Figure 3.10: Layout of Placement for Wire Mesh.

3.4 3D MODELLING

The complete geometries of the layers in the PV module and the heat sinks have been constructed in SOLIDWORKS 2019. As mentioned in Section 3.3, each layer in the PV module is considered to be a single, solid, homogenous layer of material with constant physical and thermal properties. Each layer of material has been constructed as per defined dimensions in **Table 3.1**, and then assembled to make the complete solar panel. It is ensured that the layers maintain proper contact between each other. All layers except for the heat sink are identical for every test case. Separate assemblies are made for each heat sink configuration, and finally full scale geometries have been prepared.

ANSYS software package (Version 19.2, Revision 3) has been used to perform the simulations. It is a software that leverages the method of finite element analysis (FEA) for solving the heat transfer equations for geometries being tested. As the cases are considered to be in steady state, ANSYS Steady-State Thermal is used to analyze the heat transfer in the geometries. Each layer in the PV module has its definite properties, such as specific heat, isotropic thermal conductivity and density. These physical and thermal properties of each material is set in the Engineering Data section of the ANSYS Workbench. To prepare the geometries for simulation, they are imported into ANSYS DesignModeler. As per the settings in the Engineering Data part, each layer in the model is assigned to its respective material. In order to reduce the computational load, and also leveraging the existence of perfect symmetry in the horizontal plane of the geometries, each model is reduced to 1/4th of the total size. This essentially reduces the models to now have a quarter of their lengths, widths and number of heat sinks (fifteen for L and T fins, and a quarter of total for the wire mesh) while maintaining the same total thickness. The meshing process is carried out in the ANSYS Mechanical software. The number of elements in the mesh are set such as to complete the simulation within a reasonable period of time while maintaining sufficient accuracy. Separate grid independence tests have been carried out for each geometry, which are explained in a later section. The boundary conditions are set in the respective options in the Steady-State Thermal menu, and finally the solver is launched to carry out the simulation. The end result is configured to show the PV module temperatures, heat sink temperatures and overall temperatures in tabular form as well as in visual

temperature contours. These results are used to construct several sets of graphs that can represent the trends and changes in the tested parameters.

In order to simplify the numerical model and reduce the computational effort for the simulations, a number of assumptions have been followed. The assumptions for this study are listed as follows:

- The entire simulation takes place under steady-state conditions.
- The layers of the PV module are completely solid and homogenous.
- The physical and chemical properties of the assigned materials do not change at any point in the experiment.
- The dimensions of the geometries are constant throughout.
- There is no heat generation within the PV module layers or the heat sink.
- The only incoming heat is from the solar radiation at specified amounts.
- The temperature of the whole body is same at initial condition.
- Heat transfer through convection is ignored for the edges where symmetry is applied, as those edges are actually in perfect contact in the complete geometry.
- Heat flux is considered to be incident perpendicular to the top surface of the glass cover.
- Air surrounding the PV module and heat sink is stagnant, that is, the wind velocity is zero.

As mentioned before, the heat transfer through each layer of the PV module takes place via conduction, convection and radiation. The faces through which heat transfer occurs along with their respective directions are shown in **Figure 3.11**.

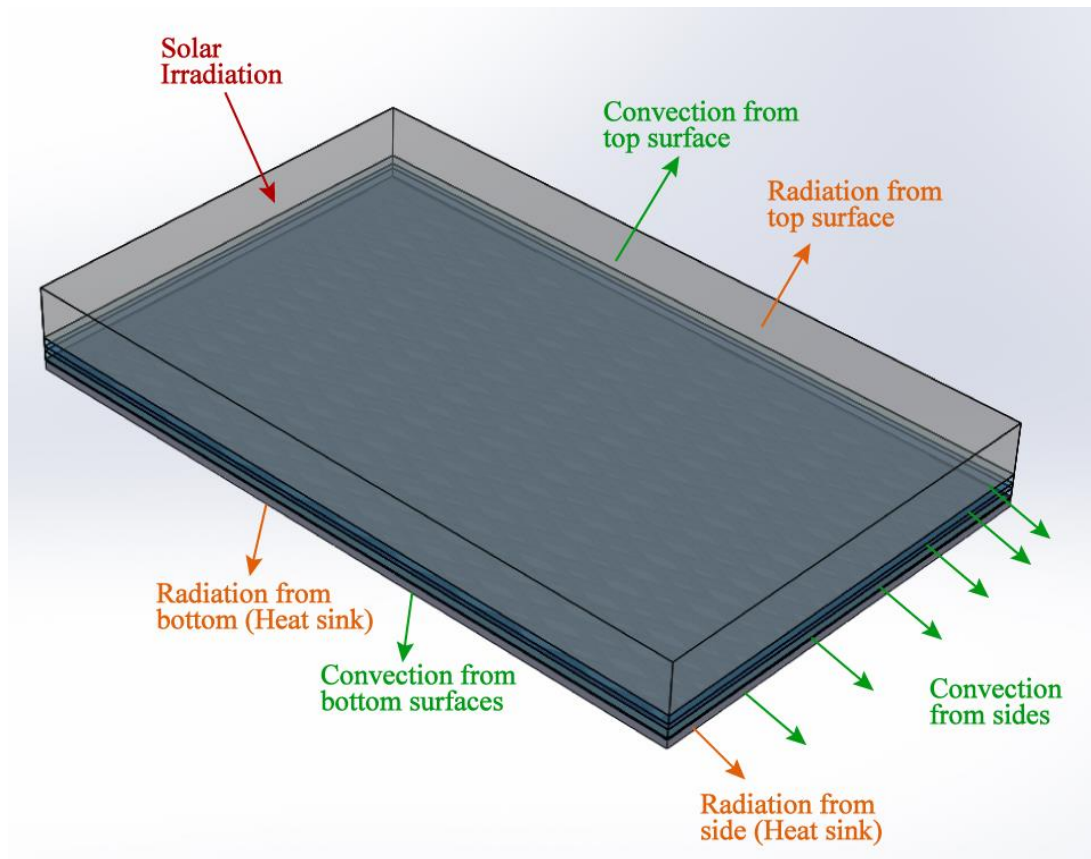


Figure 3.11: Heat Transfer Modelling for the PV Module.

3.5 GRID INDEPENDENCE TEST

The accuracy of simulation results depend on the number of elements that the numerical model has been broken down into. A smaller element size results in a greater quantity of elements. The higher the number of elements, the more accurate the end results are, because the numerical calculations are performed for much smaller sized units in the geometry. However, carrying out calculations for too many elements is demanding on the computer hardware and requires a significant amount of time for completing the simulation. Therefore, the element size needs to be chosen such that the program can produce the results within a reasonable amount of time while maintaining highest possible accuracy. In order to determine the most suitable element size, a grid independence test is carried out. The test helps to find out the difference in results when using different element sizes, so that a particular size can be chosen after which further refinement has negligible effect on the accuracy of results. At that point, it can be declared that the results are then independent of changes in the mesh, hence the grid independence is established.

To establish grid independence, each model has been tested at fixed conditions, that is, the ambient temperature and convective heat transfer coefficients have been kept the same, while the same four heat flux values have been applied for each output PV module temperature. The tests have been carried out with four element sizes differing by 0.001 m each time, starting from element size of 0.009 m, until a negligible difference in output PV module temperature has been reached. Element sizes are categorized as coarse, medium, fine and superfine, with element sizes of 0.009 m, 0.008 m, 0.007 m and 0.006 m, respectively. The meshing for the Solid T heat sink model has been shown in Figure 15. An exception is made for wire mesh where the simulation could not be successfully completed on the available hardware, in which case the superfine size category was omitted. **Table 3.3** shows the number of elements for corresponding models and sizes. Mesh size comparisons for the Solid T model have been shown in **Figure 3.12**. The chosen mesh diagrams and variations in PV module temperature for each element size in graphical forms are shown in **Figure 3.13** and **Figure 3.14**, respectively.

Table 3.3: Grid Independence Test Parameters.

Heat Sink Model	Size Category	Element Size (m)	Number of Elements
Solid L Fins	Coarse	0.009	57970
	Medium	0.008	72681
	Fine	0.007	95688
	Superfine	0.006	117403
Perforated L Fins	Coarse	0.009	104536
	Medium	0.008	118262
	Fine	0.007	138434
	Superfine	0.006	157509
Solid T Fins	Coarse	0.009	59650
	Medium	0.008	74931
	Fine	0.007	98658
	Superfine	0.006	105722
Perforated T Fins	Coarse	0.009	120042
	Medium	0.008	133673
	Fine	0.007	154250
	Superfine	0.006	160774
Wire Mesh	Coarse	0.009	45672
	Medium	0.008	56002
	Fine	0.007	70030

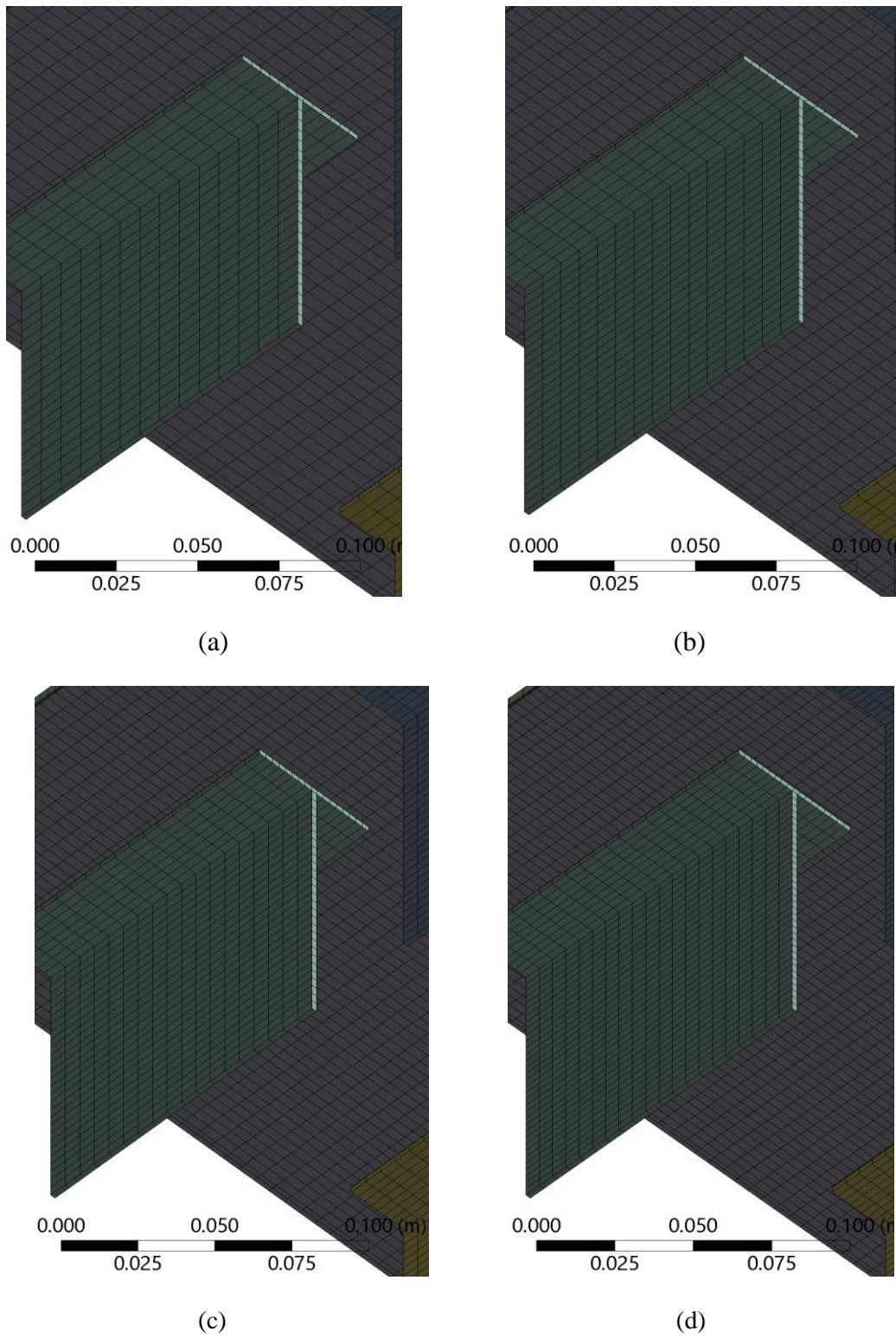


Figure 3.12: Comparison of Mesh for (a) Coarse, (b) Medium, (c) Fine and (d) Superfine Sizes for Solid T Fins.

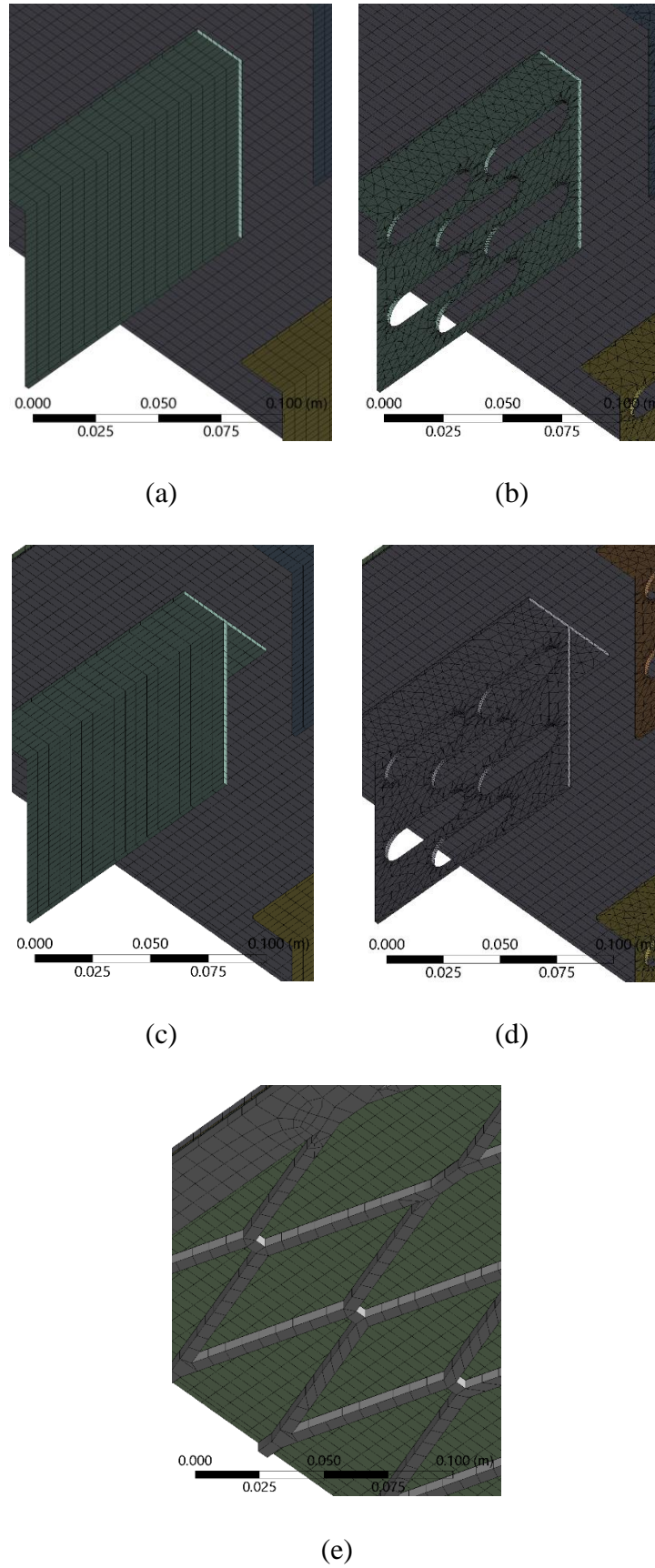


Figure 3.13: Mesh at Fine Element Size for (a) Solid L Fins, (b) Perforated L Fins, (c) Solid T Fins, (d) Perforated T Fins, and (e) Wire Mesh.

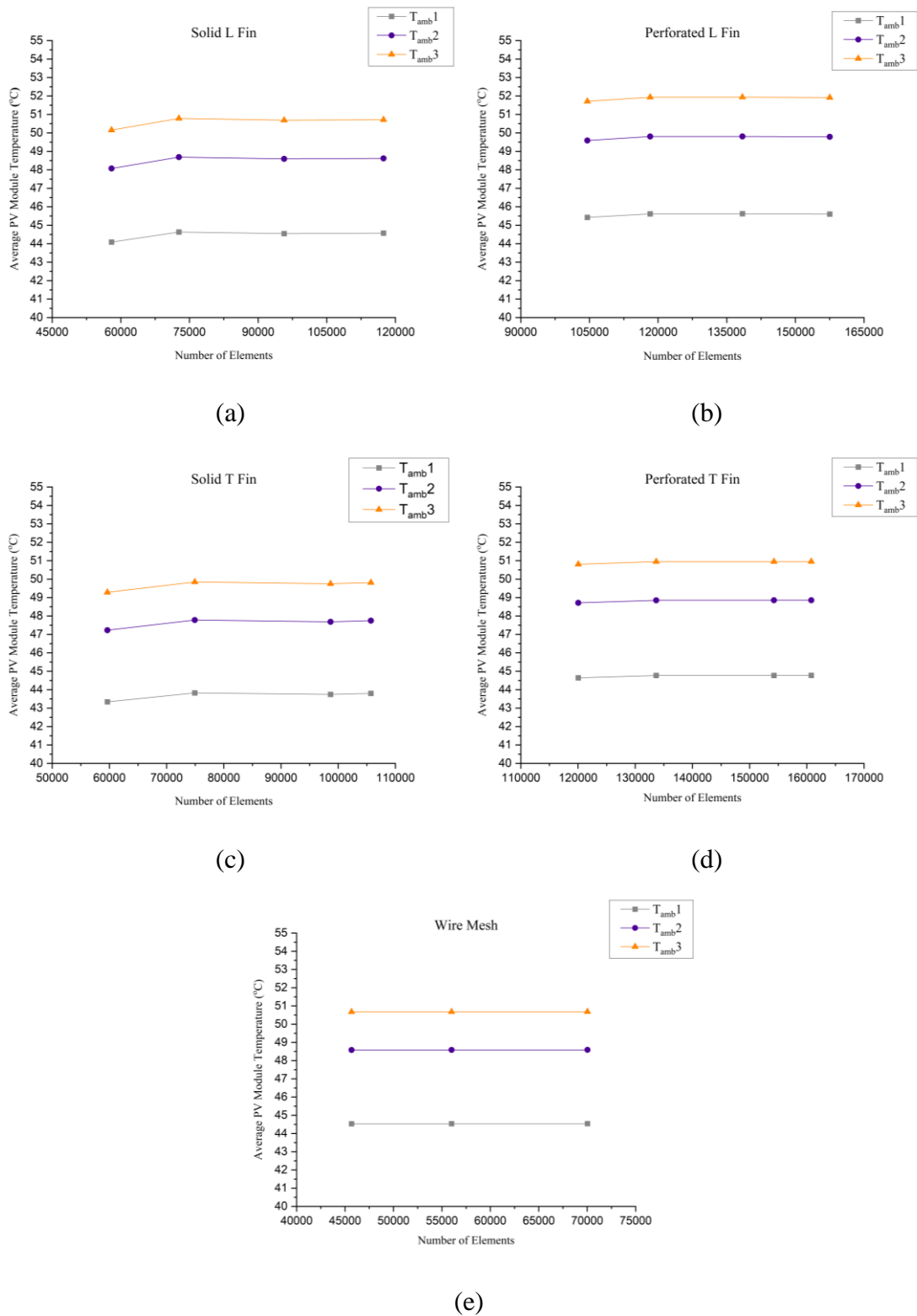


Figure 3.14: Grid Independence Tests for Solid L Fins, Perforated L Fins, Solid T Fins, Perforated T Fins, and Wire Mesh.

As seen from the graphs, the output PV module temperature hardly varies when using a mesh size of medium or better. The maximum percentage difference in PV module temperature results between fine and superfine categories for Solid L, Perforated L, Solid T and Perforated T models have been found to be 0.05%, 0.04%, 0.13% and 0.01%, respectively. For wire mesh, the difference is 0.01% between medium and fine levels. These numbers show that beyond the fine level, there is negligible difference in obtained results, which means that the results are now independent of further changes in the grid. Therefore, grid independence has been established. The decision is taken for the simulation to be run at the fine size category with element size 0.007 m for all geometries. Hence, each geometry has the number of elements corresponding to “Fine” size category as shown in **Table 3.3**. This size is chosen as appropriate for this study to achieve the maximum possible accuracy while being reasonably time efficient on the simulations.

3.6 MODEL VALIDATION

The numerical model has been compared against previous experimental data gathered by Hernandez-Perez et al. [41]. The experimental data contains ambient temperature, heat flux and resulting temperature of the PV module at 13 points of time in a day, from 6:00 AM to 6:00 PM. The geometries of the solar panel and heat sink have been created using the exact dimensions found in the paper to keep perfect consistency with the physical quantities. Furthermore, the thermo-physical properties, boundary conditions, and the PV cell characteristics have been kept unchanged. Therefore, the only remaining parameter for comparison is the resulting PV module temperature. This has been found from the simulation results and then compared with the experimental results to determine whether the difference is acceptable to validate the numerical model.

For validating the model against the experimental data, in the simulation software, element sizes for the geometries have been tested in increments of 0.001 m, starting from 0.01 m. In between element sizes 0.007 m and 0.006 m having 25253 and 33799 elements, respectively, the maximum percentage difference in results is only 0.12%. This is an acceptable point to consider that the variation in temperature is negligible for further reduction in mesh sizing. 0.006 m is chosen as the element size

for the validation simulation as it contains the highest number of elements, and it can be used to complete the numerical simulation within a reasonable amount of time. The experimental model and its meshing are shown in **Figure 3.15** and **Figure 3.16**, respectively.

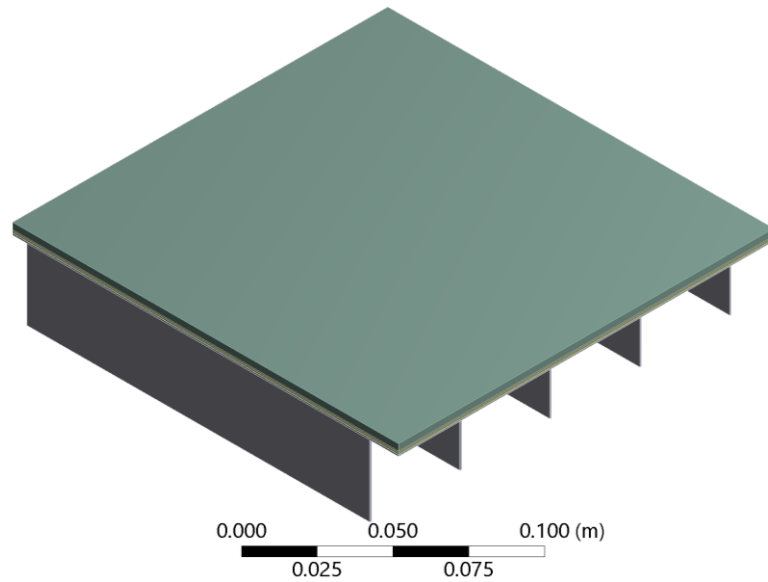


Figure 3.15: Recreation of the Experimental Model for Validation.

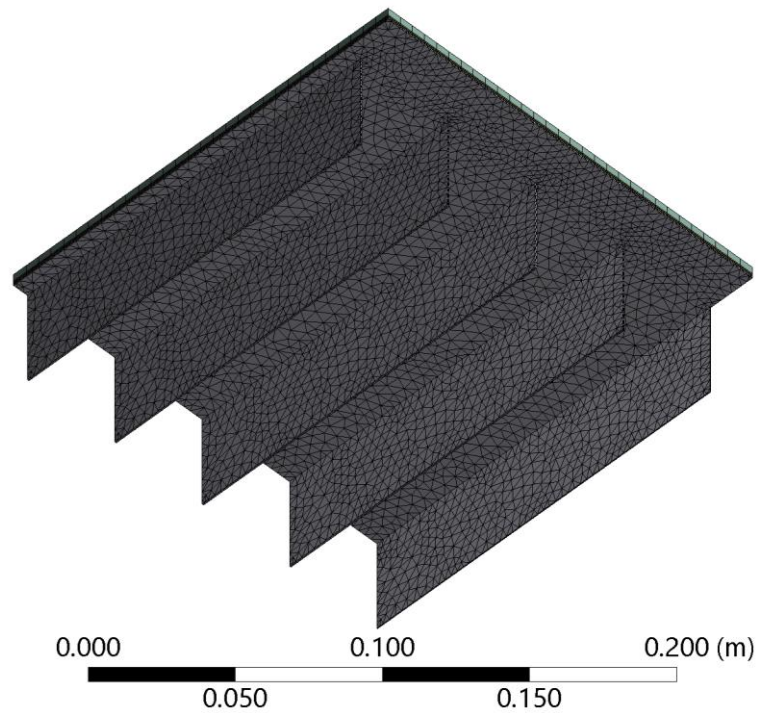


Figure 3.16: Superfine Mesh for Experimental Model with 33799 Elements.

The results from the simulation are shown along with the results from the previous experiment in **Table 3.4**. **Figure 3.17** shows a graph for the variation of both the experimental PV module temperature, T_{exp} and the simulated PV module temperature, T_{sim} at the particular time steps. From the graph, close correlation between the results can be observed. The average difference between the sets of results is found to be 3.42%. Considering that the experimental conditions may be influenced by many external factors, and the simulation takes place assuming a perfectly controlled environment, the difference in results can be considered small enough for the results to be acceptable to validate the numerical model used for the simulation.

Table 3.4: Data from Experimental Results [41] and Simulated Results.

Time of Day	Ambient Temperature, T_{amb} (°C)	Solar Radiation (W/m ²)	Experimental PV Temperature, T_{exp} (°C)	Simulated PV Temperature, T_{sim} (°C)	Percentage Error
6	22.405	0.156	22.973	22.408	2.46%
7	22.242	57.682	23.992	23.286	2.94%
8	24.203	277.718	28.497	29.229	2.57%
9	26.654	479.059	34.236	35.27	3.02%
10	28.554	648.760	37.882	40.158	6.01%
11	30.025	765.250	39.974	43.658	9.22%
12	31.517	792.575	43.513	45.602	4.80%
13	32.191	768.126	44.747	45.826	2.41%
14	33.127	673.209	45.605	45.079	1.15%
15	33.964	542.337	46.410	43.599	6.06%
16	33.740	256.146	38.150	38.322	0.45%
17	33.535	79.254	35.898	34.958	2.62%
18	32.861	5.909	33.217	32.968	0.75%
Average Percentage Error					3.42%

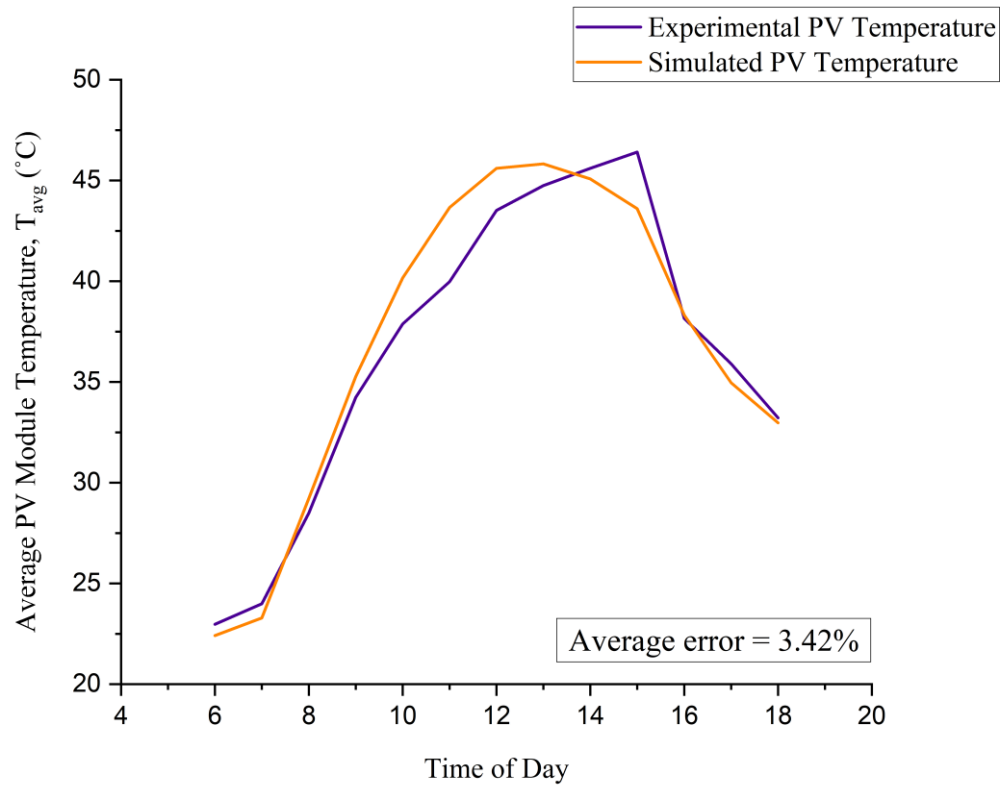


Figure 3.17: Graphical Comparison of Experimental [41] and Simulated Results.

CHAPTER FOUR

RESULTS AND DISCUSSION

4.1 FINAL SIMULATION PARAMETERS

This chapter presents the results from all the simulations carried out on the five different geometries of aluminium heat sinks designed for passively cooling solar panels. In order to produce a valid set of results from the simulations, consistent data has been used along with definite, controlled variables. For comparison of temperature reduction capabilities among the heat sink models discussed, a number of parameters have been set as control parameters in each simulation. These are discussed as follows.

The initial conditions upon which the simulations have been performed have already been listed in Chapter 3. Grid independence tests have been completed to determine the most suitable element sizing for each model, the results of which can be found in Chapter 3 as well. The initial temperature of the model has been set at 25 °C. The corresponding values for heat flux have been set in the order of 600 W/m², 800 W/m², 1000 W/m² and 1200 W/m². Once all of these considerations have been put into place, the remaining parameters are the ambient temperatures at each point of time, and the convection coefficient for heat transfer. Hence, to evaluate the performance of the heat sink geometries, the simulations have been carried out using four different values of ambient temperature, corresponding to the heat flux, and three different values for the convection coefficient. Resulting PV module temperatures for each model have been evaluated using ambient temperatures of 25 °C, 30 °C, 35 °C and 40 °C, and convection coefficients of 8 W/m²K, 12 W/m²K and 16 W/m²K.

4.2 RESULTS, ANALYSIS AND DISCUSSION

After performing numerical simulation on each model under specific parameters at steady-state condition, the results have been acquired and presented in tabular and graphical forms. The main output parameter is the resulting PV module temperature for each ambient temperature and convection coefficient. From **Table 4.1** to **Table 4.5** and **Figure 4.1** to **Figure 4.5** the results are shown for each model.

Table 4.1: Simulation Results for Solid L Fins.

Heat Transfer Coefficient, h_c (W/m ² K)	Ambient Temperature, T_{amb} (°C)	Minimum PV Module Temperature, T_{min} (°C)	Maximum PV Module Temperature, T_{max} (°C)	Average PV Module Temperature, T_{avg} (°C)
8	25	39.659	51.22	46.924
	30	48.916	63.5	58.218
	35	58.193	75.929	69.574
	40	67.29	87.985	80.652
12	25	34.534	44.481	41.12
	30	42.479	55.344	51.062
	35	50.4	66.194	60.975
	40	58.238	76.847	70.743
16	25	31.848	40.571	37.826
	30	39.02	50.426	46.871
	35	46.168	60.24	55.877
	40	53.271	69.934	64.795

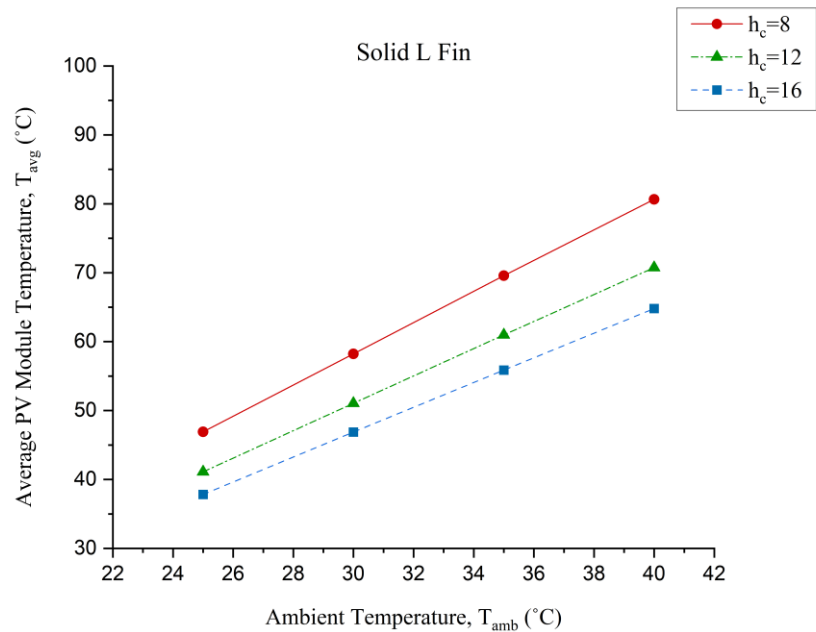


Figure 4.1: Average PV Module Temperature VS Ambient Temperature at Different Convection Coefficients for Solid L Fins.

Table 4.2: Simulation Results for Perforated L Fins.

Heat Transfer Coefficient, h_c (W/m ² K)	Ambient Temperature, T_{amb} (°C)	Minimum PV Module Temperature, T_{min} (°C)	Maximum PV Module Temperature, T_{max} (°C)	Average PV Module Temperature, T_{avg} (°C)
8	25	44.063	51.614	48.5
	30	54.484	63.942	60.129
	35	64.971	76.442	71.858
	40	75.206	88.555	83.271
12	25	38.252	44.7	42.229
	30	47.301	55.608	52.465
	35	56.326	66.508	62.679
	40	65.226	77.205	72.729
16	25	35.053	40.709	38.655
	30	43.216	50.598	47.94
	35	51.348	60.448	57.185
	40	59.409	70.174	66.332

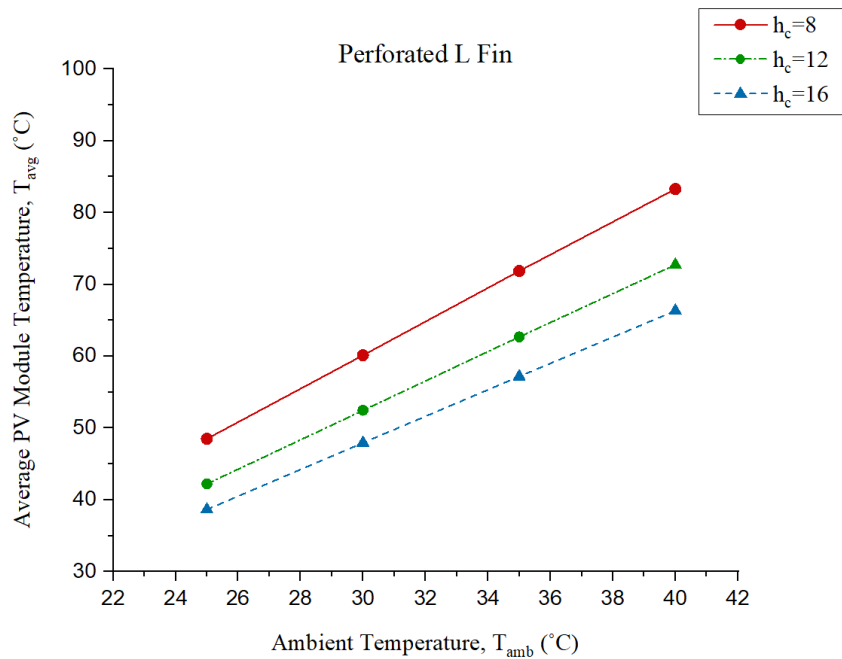


Figure 4.2: Average PV Module Temperature VS Ambient Temperature at Different Convection Coefficients for Perforated L Fins.

Table 4.3: Simulation Results for Solid T Fins.

Heat Transfer Coefficient, h_c (W/m ² K)	Ambient Temperature, T_{amb} (°C)	Minimum PV Module Temperature, T_{min} (°C)	Maximum PV Module Temperature, T_{max} (°C)	Average PV Module Temperature, T_{avg} (°C)
8	25	40.912	48.774	45.912
	30	50.563	60.626	56.992
	35	60.23	72.541	68.107
	40	69.706	84.161	78.97
12	25	35.658	42.946	40.317
	30	43.961	53.455	50.046
	35	52.236	63.929	59.741
	40	60.422	74.244	69.306
16	25	32.85	39.565	37.166
	30	40.345	49.157	46.021
	35	47.813	58.704	54.836
	40	55.231	68.152	63.573

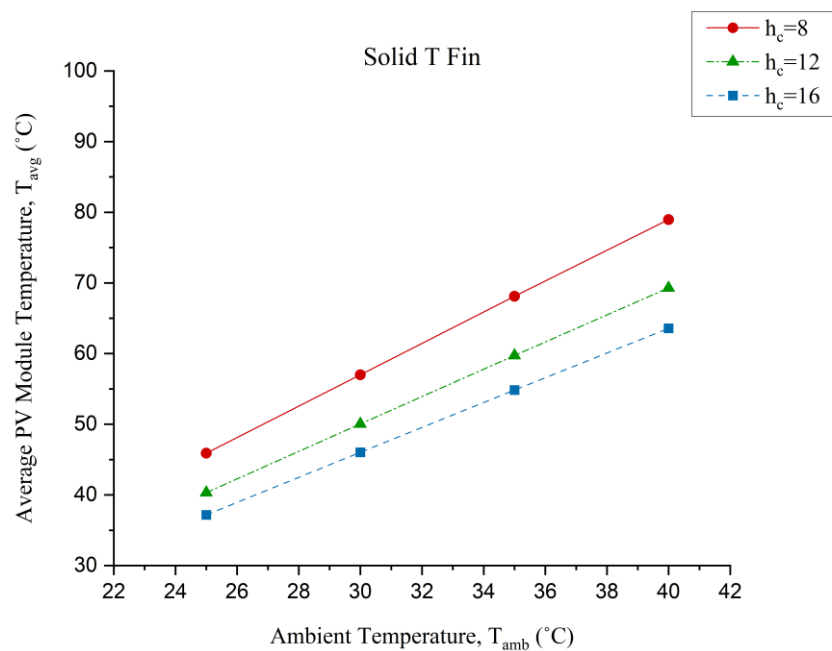


Figure 4.3: Average PV Module Temperature VS Ambient Temperature at Different Convection Coefficients for Solid T Fins.

Table 4.4: Simulation Results for Perforated T fins.

Heat Transfer Coefficient, h_c (W/m ² K)	Ambient Temperature, T_{amb} (°C)	Minimum PV Module Temperature, T_{min} (°C)	Maximum PV Module Temperature, T_{max} (°C)	Average PV Module Temperature, T_{avg} (°C)
8	25	44.971	49.303	47.43
	30	55.694	61.231	58.846
	35	66.474	73.24	70.33
	40	76.997	84.933	81.526
12	25	39.077	43.16	41.379
	30	48.397	53.706	51.397
	35	57.689	64.223	61.385
	40	66.856	74.574	71.226
16	25	35.815	39.626	37.955
	30	44.232	49.228	47.041
	35	52.614	58.786	56.087
	40	60.923	68.241	65.045

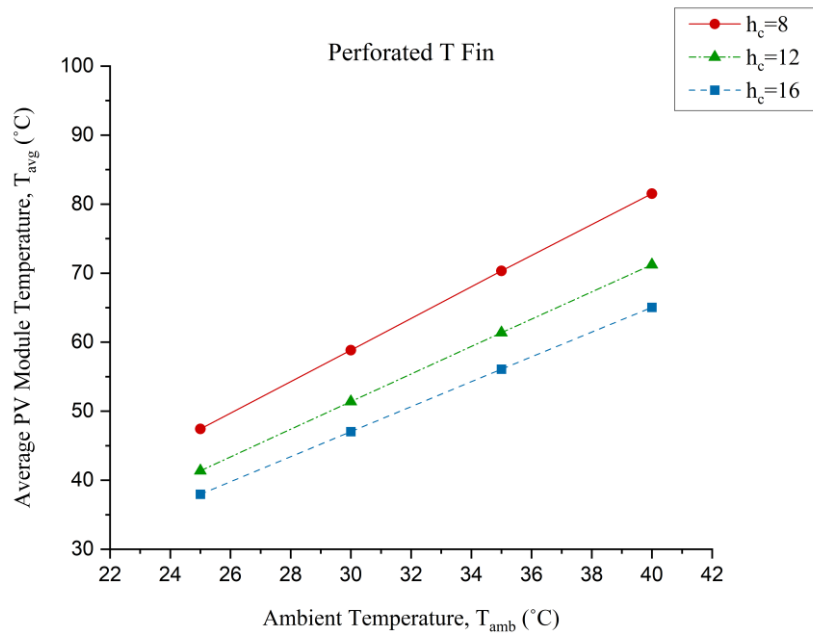


Figure 4.4: Average PV Module Temperature VS Ambient Temperature at Different Convection Coefficients for Perforated T Fins.

Table 4.5: Simulation Results for Wire Mesh.

Heat Transfer Coefficient, h_c (W/m ² K)	Ambient Temperature, T_{amb} (°C)	Minimum PV Module Temperature, T_{min} (°C)	Maximum PV Module Temperature, T_{max} (°C)	Average PV Module Temperature, T_{avg} (°C)
8	25	52.327	57.918	56.069
	30	65.816	73.025	70.651
	35	78.386	86.898	84.113
	40	90.498	100.17	97.025
12	25	44.959	50.353	48.594
	30	56.334	63.381	61.088
	35	67.244	75.728	72.977
	40	77.906	87.718	84.546
16	25	40.774	46.025	44.315
	30	50.556	57.224	55.063
	35	60.319	68.439	65.812
	40	69.93	79.415	76.352

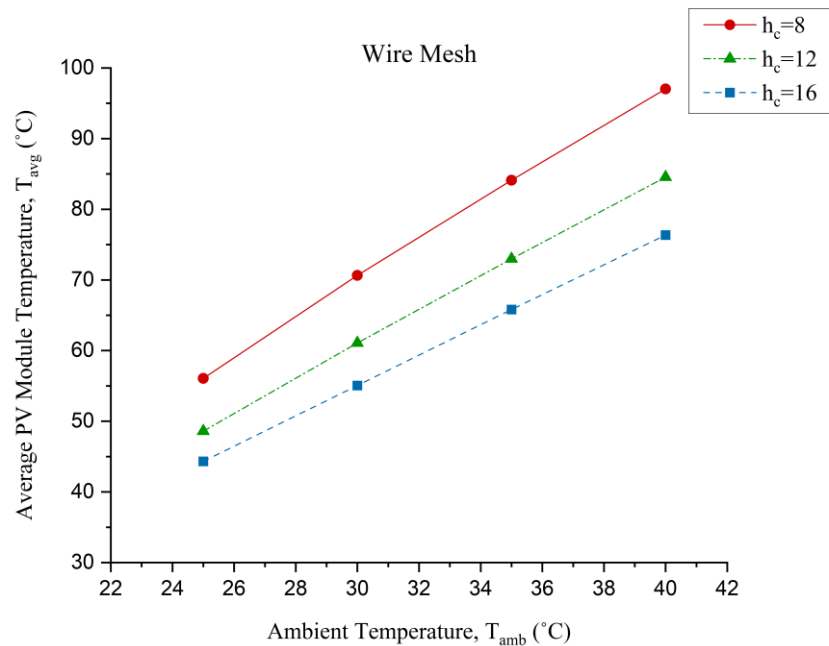


Figure 4.5: Average PV Module Temperature VS Ambient Temperature at Different Convection Coefficients for Wire Mesh.

As it can be seen from the tables, there is a total of twelve resulting average PV module temperature sets for each model, where each of the three values of h_c produces four results for four corresponding values of T_{amb} . The average PV module temperature, T_{avg} along with T_{min} and T_{max} are shown for each corresponding T_{amb} and h_c . The results from the tables show the exact values for PV module temperatures found at the end of each simulation. Difference between the temperature extremes for each case can be calculated directly from the tables themselves. For instance, the maximum temperature difference in the PV module temperature at $h_c = 8 \text{ W/m}^2\text{K}$ and $T_{amb} = 35 \text{ }^\circ\text{C}$ when using the solid T fin is $12.31 \text{ }^\circ\text{C}$. Following are the findings from the tabular results:

- Minimum Temperature = $31.848 \text{ }^\circ\text{C}$ for Solid L fins at $h_c = 16 \text{ W/m}^2\text{K}$, $T_{amb} = 25 \text{ }^\circ\text{C}$
- Maximum Temperature = $100.17 \text{ }^\circ\text{C}$ for Wire Mesh at $h_c = 8 \text{ W/m}^2\text{K}$, $T_{amb} = 40 \text{ }^\circ\text{C}$
- Lowest average temperature = $37.166 \text{ }^\circ\text{C}$ for Solid T fins at $h_c = 16 \text{ W/m}^2\text{K}$, $T_{amb} = 25 \text{ }^\circ\text{C}$
- Highest average temperature = $97.025 \text{ }^\circ\text{C}$ for Wire Mesh at $h_c = 8 \text{ W/m}^2\text{K}$, $T_{amb} = 40 \text{ }^\circ\text{C}$

Graphs from **Figure 4.1** to **Figure 4.5** display T_{amb} on the horizontal axis, while values for T_{avg} are shown on the vertical axis. Each graph combines the results for different values of h_c to show the effectiveness of the respective heat sink model. Each line represents the variation of T_{avg} with T_{amb} at a fixed value for h_c , so there are three lines for three corresponding values of h_c on each graph. As expected, the graphs show higher T_{avg} at higher values of T_{amb} and lower h_c . The highest T_{avg} can be seen at lowest h_c values for every heat sink design, indicating the lowest cooling performance. From the graphs, it is evident that all of the models show greater reduction in T_{avg} at higher values of h_c . The gradient of the lines for each model is almost constant, hence a linear relationship between T_{avg} and T_{amb} can be seen from the resulting graphs for every heat sink model. The trend in the graphs imply that the difference between the values of T_{avg} increases as the lines move towards the right, i.e. as T_{amb} increases further. The lines can be extrapolated to clearly see the pattern. This can be considered as expected behavior as higher h_c implies greater rate of heat transfer by convection according to

Newton's Law of Cooling. Therefore the simulation results can be considered to be in agreement with the theoretical prediction. The vertical difference between any two lines shows the difference in T_{avg} for different h_c at the same T_{amb} . This gives a good insight into the performance difference of the heat sink for various values of h_c . The difference in T_{avg} between $h_c = 8 \text{ W/m}^2\text{K}$ and $h_c = 12 \text{ W/m}^2\text{K}$ is greater than that between $h_c = 12 \text{ W/m}^2\text{K}$ and $h_c = 16 \text{ W/m}^2\text{K}$. This indicates a non-linear relationship between h_c and T_{avg} . There are only three points on the graph for h_c and T_{avg} at each T_{amb} , so a better insight on the relationship could be obtained from a larger number of points. The same can be said for heat flux, as T_{amb} increases in tandem with the heat flux. The reason for the linearity can be attributed to the fact that all the dynamic variables, such as those related to the working environment, are considered to have negligible effect on the tests here as per the methodology of this work. In the event where such variables are considered, the linear relationship between T_{avg} and T_{amb} may not hold true. However, for the purpose of this study, it is imperative to keep random variables out of consideration to compare the performances of the heat sinks under perfect conditions. The results shown in the graphs encompass results from using heat flux values starting from 600 W/m^2 up to 1200 W/m^2 . For the purpose of a realistic assumption, the values close to the practical occurrences need to be chosen. On a regular day, the average incoming solar radiation hovers around 800 W/m^2 in the noon [42]. Based on this fact, comparison of results at this value of heat flux can be considered to reflect close to practical expectations for the output of these heat sinks. The graph in **Figure 4.6** shows the variation of T_{avg} against solar radiation at a fixed value of T_{amb} for different h_c when using Solid T fins. The value of T_{amb} is set at $25 \text{ }^\circ\text{C}$. The relationship between T_{avg} and Solar Radiation is linear, and as the h_c is increased, the gradient decreases. This implies that as the solar radiation increases, the rate of increase of T_{avg} gets smaller at higher h_c . Therefore, at lower values of h_c , the values for T_{avg} will increase in larger increments with increasing solar radiation. The variation of T_{avg} against solar radiation at a fixed value of h_c for different T_{amb} is shown in **Figure 4.7** when using Solid T fins. In this case, the value of h_c is set at $12 \text{ W/m}^2\text{K}$. Upon observation from the graph, it can be seen that T_{avg} increases linearly with increasing solar radiation. The increase in T_{avg} with increasing T_{amb} also appears to have a linear relationship, as observed by the vertical difference between the points at each step of solar radiation. It can be deduced that at a fixed value of h_c , the increase in T_{avg} is directly proportional to the solar radiation.

Furthermore, increase in T_{avg} is also directly proportional to T_{amb} when considering the same value of solar radiation.

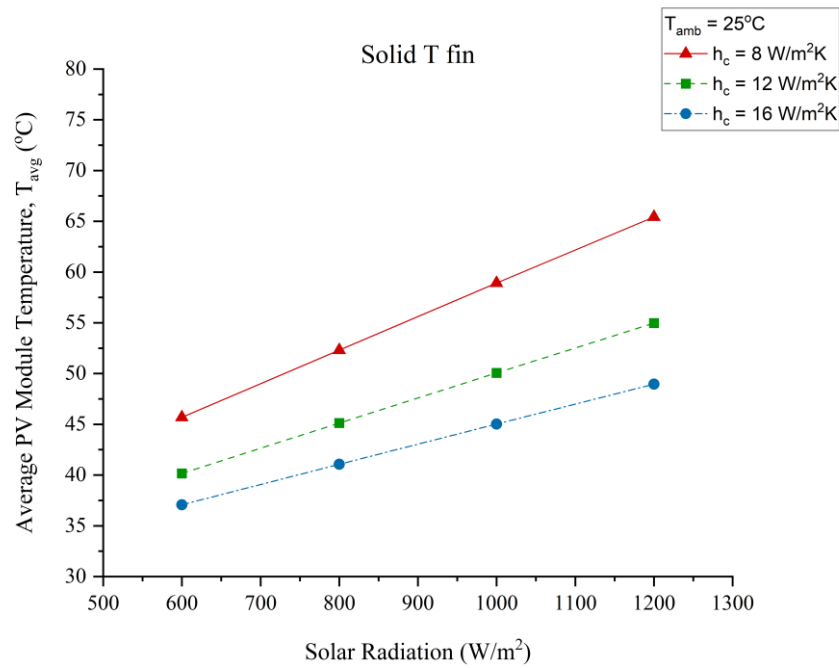


Figure 4.6: Average PV Module Temperature VS Solar Radiation at Fixed Ambient Temperature and Different Convection Coefficients for Solid T Fins.

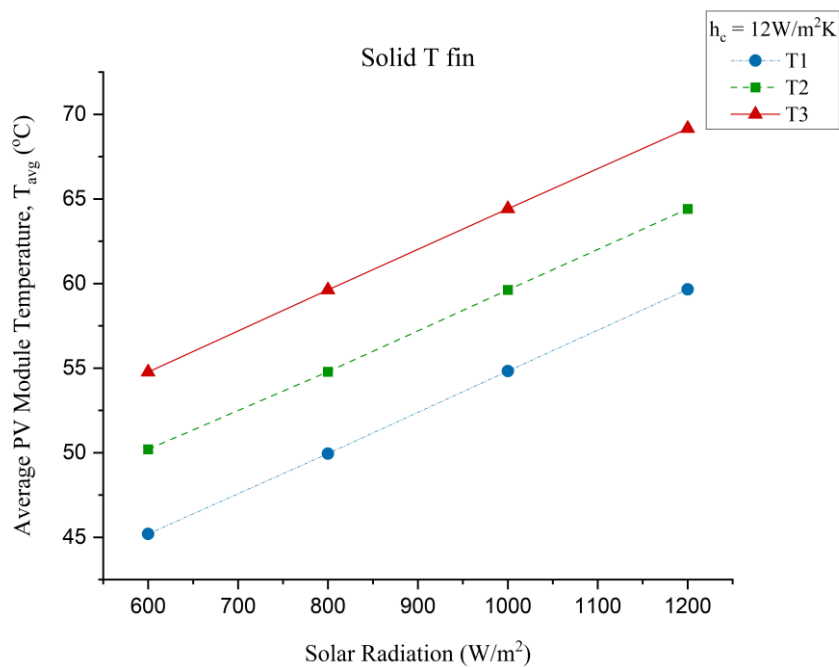


Figure 4.7: Average PV Module Temperature VS Solar Radiation at Fixed Convection Coefficient and Different Ambient Temperatures for Solid T Fins.

The results shown from **Figure 4.8** to **Figure 4.17** present the temperature contours from the simulations that have been carried out for the performance tests of all five heat sink models. The temperature contours help to visualize the minimum to maximum temperature distribution throughout the PV module for a particular step, allowing to see the areas where heat may be concentrated, or regions where the highest amount of cooling takes place. Color spectrum for the contours have been set from blue to red with labelled temperature values, indicating the minimum PV module temperature, T_{min} , at the blue end and maximum PV module temperature, T_{max} , at the red end. The unit for temperature is in degrees Celsius ($^{\circ}\text{C}$). The ambient temperature, T_{amb} , and corresponding heat flux are $30\text{ }^{\circ}\text{C}$ and 800 W/m^2 , respectively. Some general trends can be easily identified from the image results. In the temperature contours, the temperature of the PV module is the lowest at the point of contact between the tedlar and heat sink, indicated by blue regions. Moving further away from the point of contact, the temperature of the PV module starts to rise, as shown by the color changing to yellow, orange, and then finally to red. The top and bottom sides of the PV module have the same pattern of temperature distribution, although at different ranges. This is because the upper surface is directly exposed to the heat flux, resulting in maximum heat absorption at that particular face and a temperature band weighted more towards red. The lower face of the PV module, i.e. the tedlar is not facing the sun, hence it has a band of temperature closer to the blue spectrum. The temperature distribution can be seen as following a pattern owing to the positioning of the heat sinks. For the first four types of heat sinks, the temperature distribution is in a pattern following the arrangement of the heat sinks. Green and blue contours on the PV module indicate the spots where the heat sinks are adhered, indicating the highest reduction of temperature at those spots. The red regions show the areas where the heat dissipation is insufficient, resulting in highest of the temperatures across the entire model. An interesting outcome for the Wire Mesh can be seen, where the thick rectangular edges end up being the most effective regions for heat dissipation instead of the main mesh. This happens due to the direct contact of the thick edges to the PV module, so there is a large area for dissipating heat through conduction. Streaks of red areas can be observed in between the gaps of heat sinks. This behavior suggests that the heat transfer may be much more effective when the gaps between the heat sinks are reduced, i.e. a larger area of the heat sink is in contact with the PV module. However, the downside to making such a design requires a greater volume of heat sink material, which ends up increasing the mass of

the solar panel and incurs a significant cost. Therefore, the price-to-performance ratio is not very feasible when contemplating a design like that. One of the issues discussed back in Chapter 2 is the material deformation of the PV layers due to temperature fluctuations and uneven temperature distribution, which can be seen on the temperature contours. In practical situation, the heat flux can vary over a large range. In that case, using a heat sink that provides uneven temperature distribution may prove to be damaging for the PV structure over time. The Solid L and Perforated L fins show the highest fluctuations of temperature over the PV module, followed by Solid T and Perforated T fins, and finally Wire Mesh.

C: Solid L Fin, Convection Coefficient 12

PV Module Temperature

Type: Temperature

Unit: °C

Time: 2

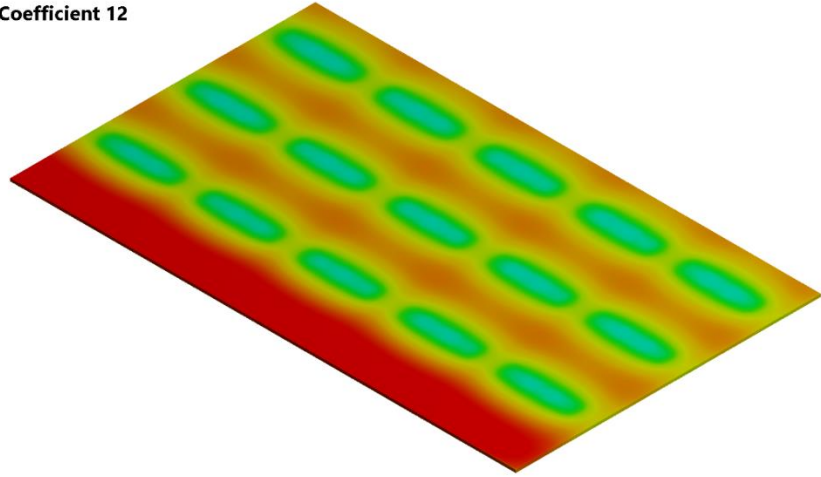
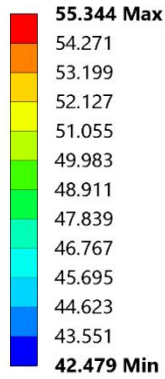


Figure 4.8: Temperature Contour for PV Module only at Ambient Temperature of 30 °C, Heat Flux of 800 W/m² and Convection Coefficient of 12 W/m²K for Solid L Fins.

C: Solid L Fin, Convection Coefficient 12

Heat Sink Temperature

Type: Temperature

Unit: °C

Time: 2

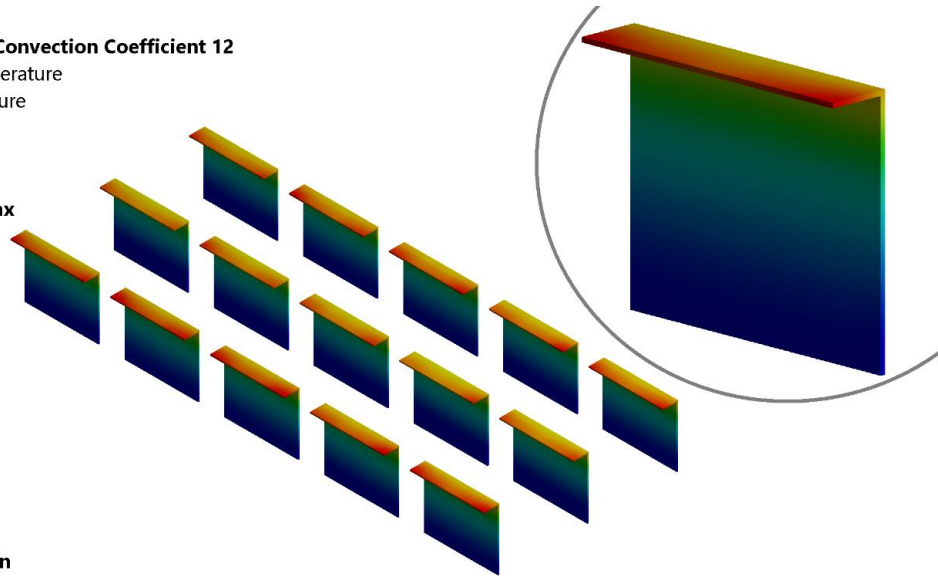
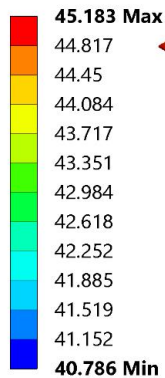


Figure 4.9: Temperature Contour for Solid L Fins at Ambient Temperature of 30 °C, Heat Flux of 800 W/m² and Convection Coefficient of 12 W/m²K.

C: Perforated L Fin, Convection Coefficient 12

PV Module Temperature

Type: Temperature

Unit: °C

Time: 2

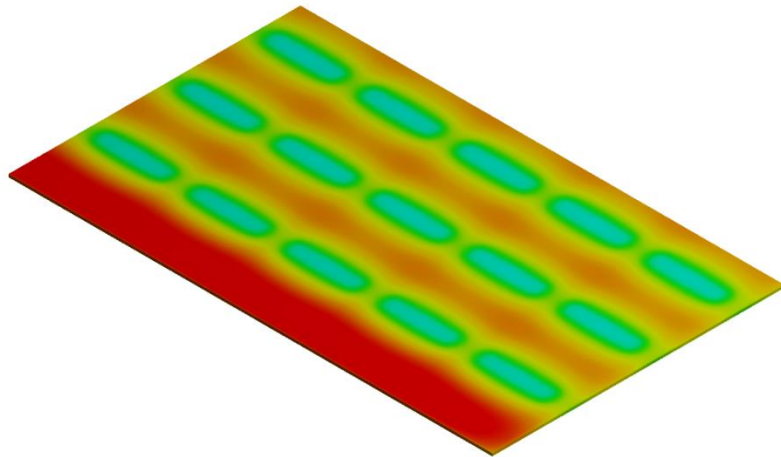
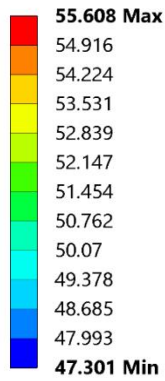


Figure 4.10: Temperature Contour for PV Module only at Ambient Temperature of 30 °C, Heat Flux of 800 W/m² and Convection Coefficient of 12 W/m²K for Perforated L Fins.

C: Perforated L Fin, Convection Coefficient 12

Heat Sink Temperature

Type: Temperature

Unit: °C

Time: 2

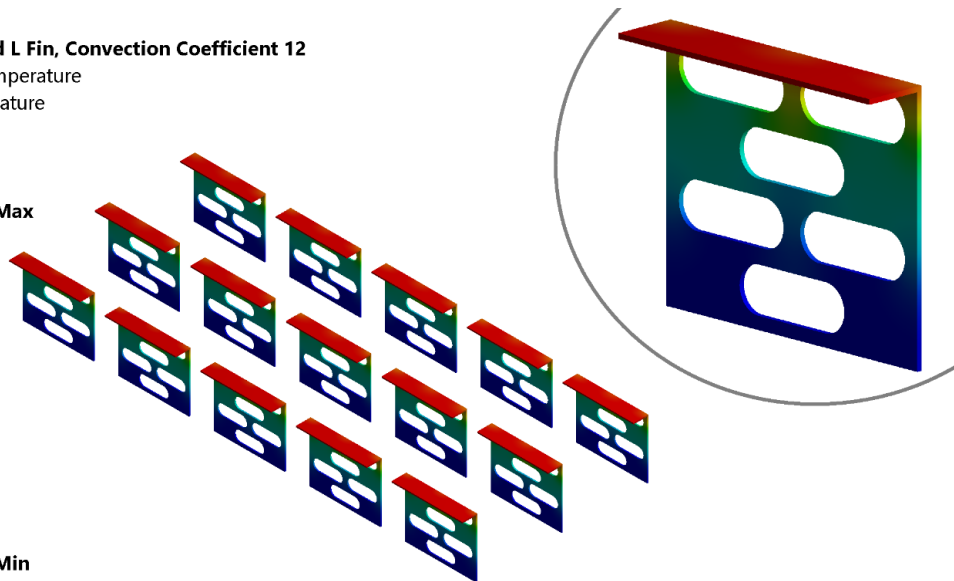
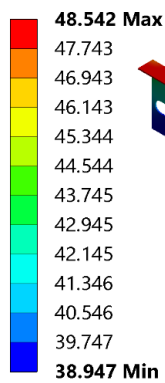


Figure 4.11: Temperature Contour for Perforated L Fins at Ambient Temperature of 30 °C, Heat Flux of 800 W/m² and Convection Coefficient of 12 W/m²K.

H: Solid T Fin, Convection Coefficient 12

PV Module Temperature

Type: Temperature

Unit: °C

Time: 2

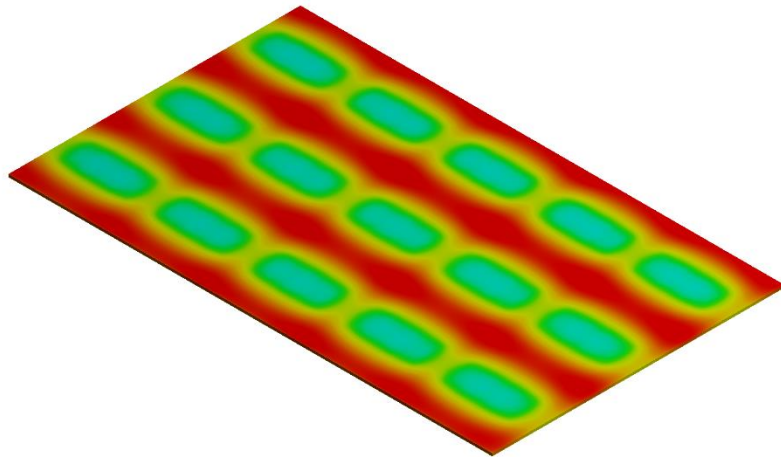
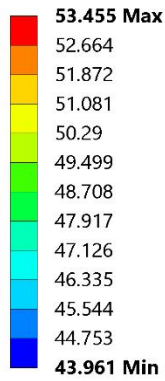


Figure 4.12: Temperature Contour for PV Module only at Ambient Temperature of 30 °C, Heat Flux of 800 W/m² and Convection Coefficient of 12 W/m²K for Solid T Fins.

H: Solid T Fin, Convection Coefficient 12

Heat Sink Temperature

Type: Temperature

Unit: °C

Time: 2

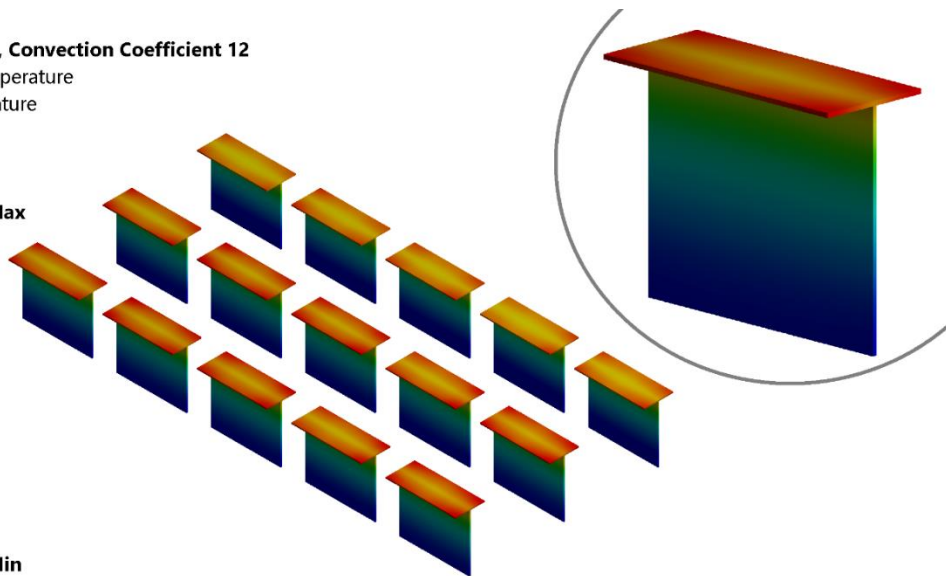
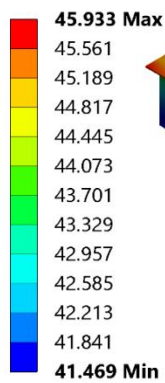


Figure 4.13: Temperature Contours for Solid T Fins at Ambient Temperature of 30 °C, Heat Flux of 800 W/m² and Convection Coefficient of 12 W/m²K.

C: Perforated T Fin, Convection Coefficient 12

PV Module Temperature

Type: Temperature

Unit: °C

Time: 2

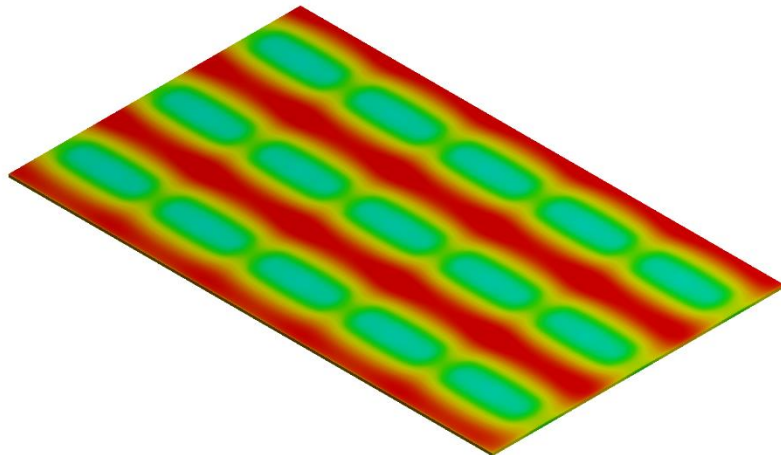
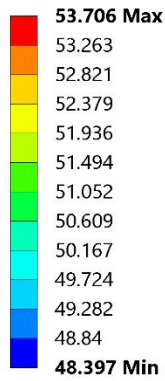


Figure 4.14: Temperature Contour for PV Module only at Ambient Temperature of 30 °C, Heat Flux of 800 W/m² and Convection Coefficient of 12 W/m²K for Perforated T Fins.

C: Perforated T Fin, Convection Coefficient 12

Heat Sink Temperature

Type: Temperature

Unit: °C

Time: 2

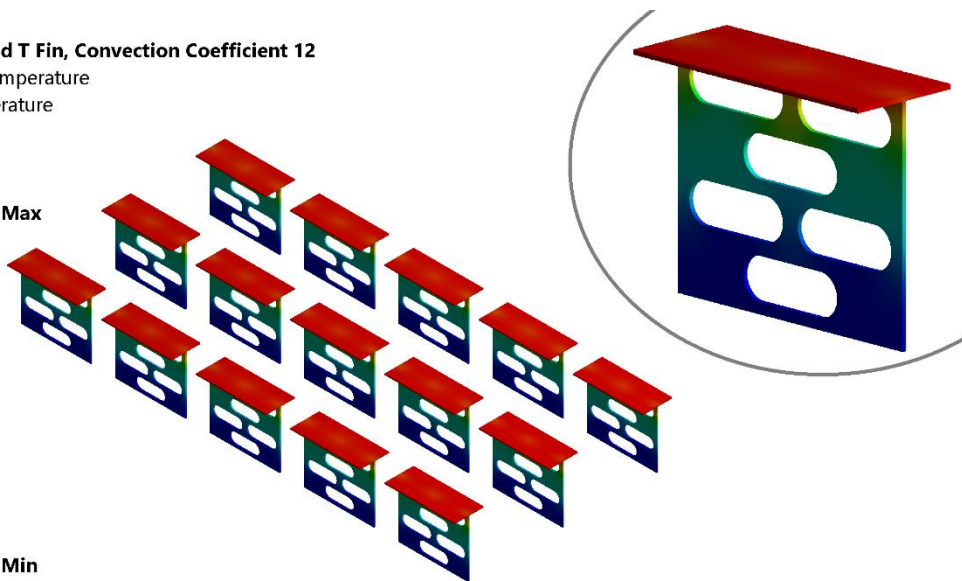
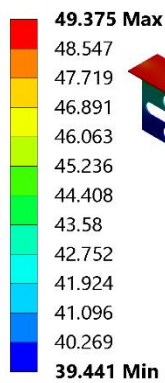


Figure 4.15: Temperature Contour for Perforated T Fins at Ambient Temperature of 30 °C, Heat Flux of 800 W/m² and Convection Coefficient of 12 W/m²K.

C: Wire Mesh, Convection Coefficient 12

PV Module Temperature

Type: Temperature

Unit: °C

Time: 2

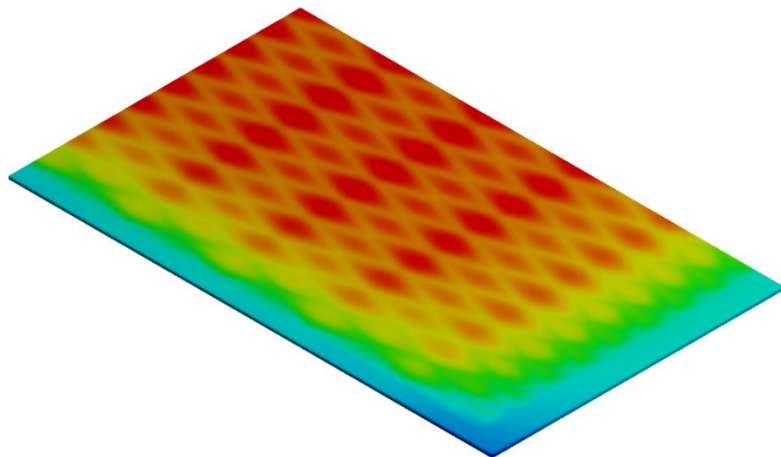
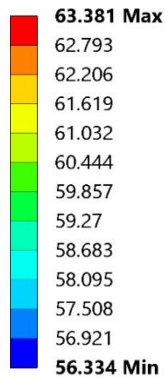


Figure 4.16: Temperature Contour for PV Module only at Ambient Temperature of 30 °C, Heat Flux of 800 W/m² and Convection Coefficient of 12 W/m²K for Wire Mesh.

C: Wire Mesh, Convection Coefficient 12

Heat Sink Temperature

Type: Temperature

Unit: °C

Time: 2

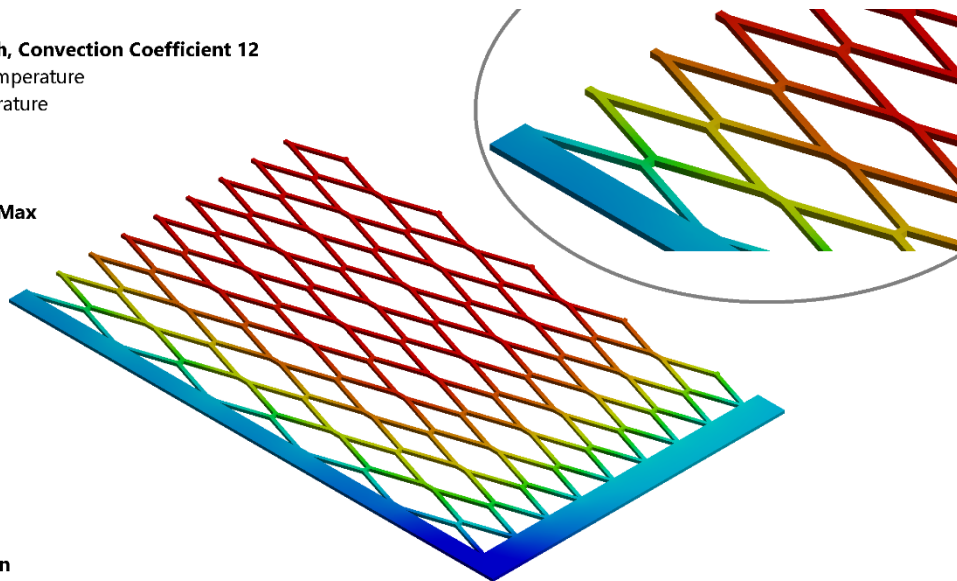
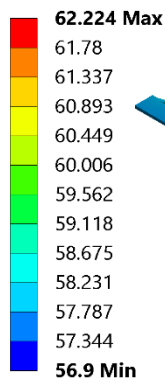


Figure 4.17: Temperature Contour for Wire Mesh at Ambient Temperature of 30 °C, Heat Flux of 800 W/m² and Convection Coefficient of 12 W/m²K.

The comparison of T_{avg} values for all models at fixed values of h_c can be used to easily identify the best performing model. Three separate graphs for T_{avg} against T_{amb} at three fixed values of h_c are shown from **Figure 4.18** to **Figure 4.20** . By measuring the vertical distance among the lines at any point, very little difference is seen among the first four types of heat sink geometry. The vertical distance between the lines increases for higher values of T_{amb} , which can be confirmed by extrapolation of the lines towards the right. That means the difference among the performances of heat sink geometries become much more apparent at significantly higher levels of T_{amb} . Hence a divergent pattern is formed from the extension of the lines. At higher values of h_c , the vertical difference between the lines decrease, bringing the lines closer to each other. This implies that at higher h_c values, the heat transfer rate for the heat sink geometries are closer to each other than before. At the same time, it also shows that the performance differences can be better examined at lower h_c values.

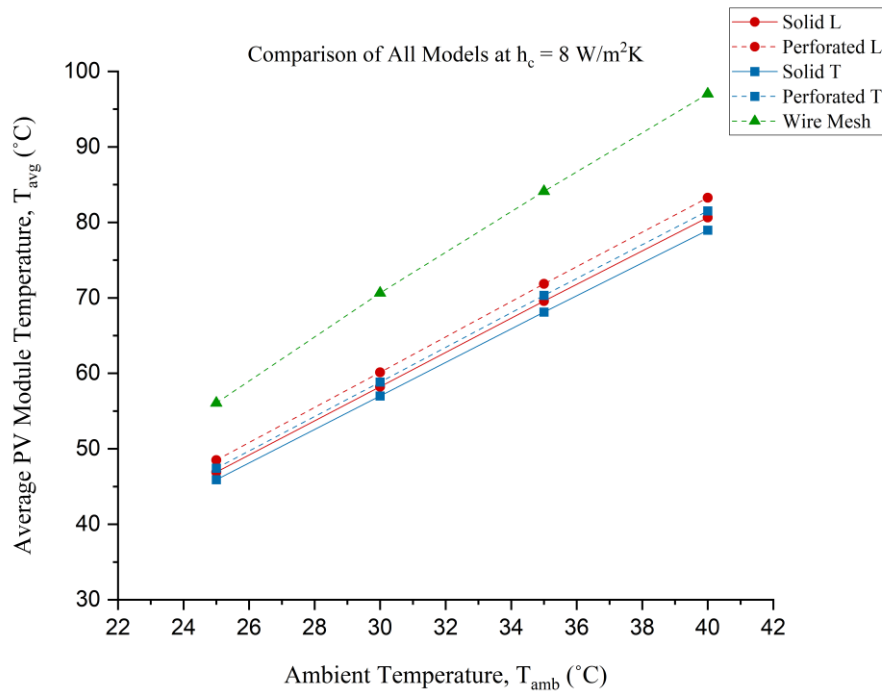


Figure 4.18: Comparison of All Heat Sink Models at Convection Coefficient of 8 W/m^2K .

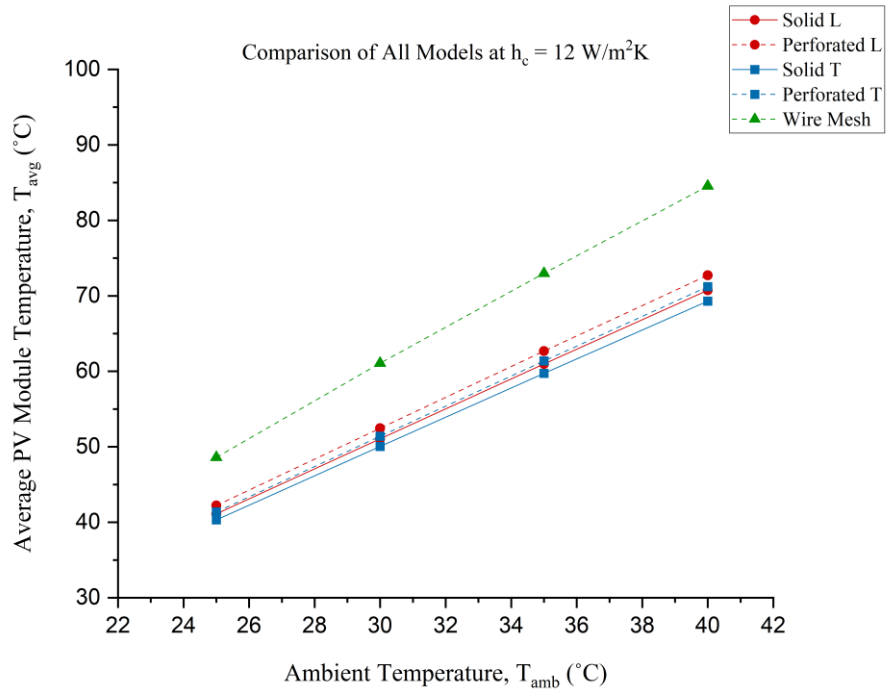


Figure 4.19: Comparison of All Heat Sink Models at Convection Coefficient of 12 $\text{W/m}^2\text{K}$.

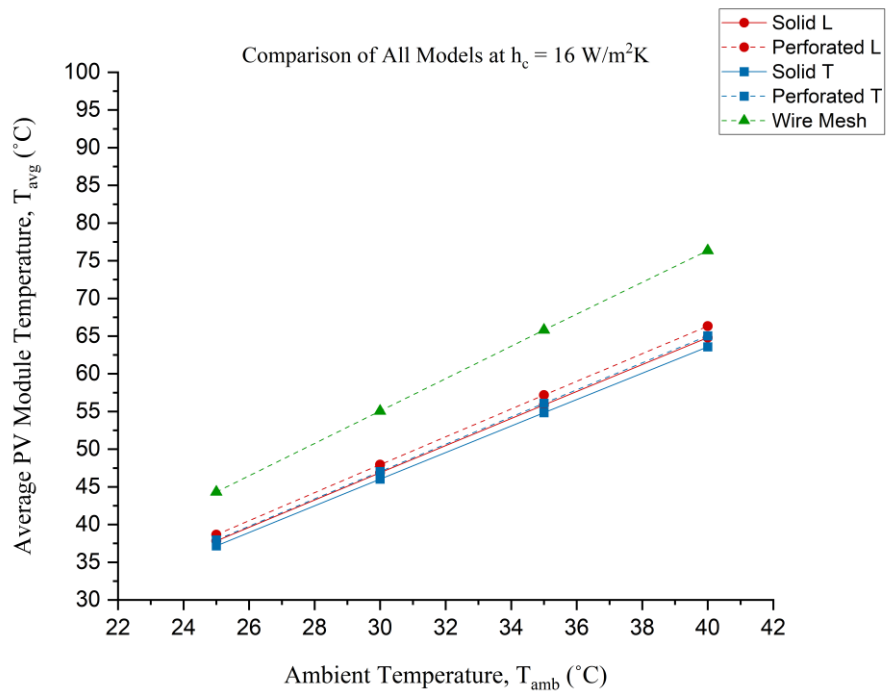


Figure 4.20: Comparison of All Heat Sink Models at Convection Coefficient of 16 $\text{W/m}^2\text{K}$.

It can be clearly seen that L and T variants from the heat sink models are better at maintaining lower T_{avg} throughout the simulations. Observing from **Figure 4.18**, at the maximum end of the values obtained, i.e. at $T_{amb} = 40\text{ }^{\circ}\text{C}$ and $h_c = 8\text{ W/m}^2\text{K}$, the value of T_{avg} for Solid T fins is $78.97\text{ }^{\circ}\text{C}$. Under the exact same conditions, the values of T_{avg} for Solid L fins, Perforated L fins, Perforated T fins and Wire Mesh are $80.652\text{ }^{\circ}\text{C}$, $83.271\text{ }^{\circ}\text{C}$, $81.526\text{ }^{\circ}\text{C}$ and $97.025\text{ }^{\circ}\text{C}$, respectively. Therefore, Solid T fins provide lower temperatures than Solid L fins, Perforated L fins, Perforated T fins and Wire Mesh by $1.682\text{ }^{\circ}\text{C}$, $4.301\text{ }^{\circ}\text{C}$, $2.556\text{ }^{\circ}\text{C}$ and $18.055\text{ }^{\circ}\text{C}$, respectively. These results are displayed comparatively in **Figure 4.21**. In terms of relative performance, this translates to lower temperatures by 2.08%, 3.14%, 5.17% and 18.6%. Similar magnitudes of difference in T_{avg} can be seen for the rest of the graph. From the observation of the other two graphs for constant h_c , it can be concluded that Solid T fins provide the lowest T_{avg} values across all three values of h_c . The reason for this may be the greater contact surface of the upper side of the fin to the PV module. Solid L fins come to a close second in the comparison, followed very closely by Perforated T fins. The line for Perforated L fins lies slightly above, while the line for Wire Mesh is evidently much higher in the graph.

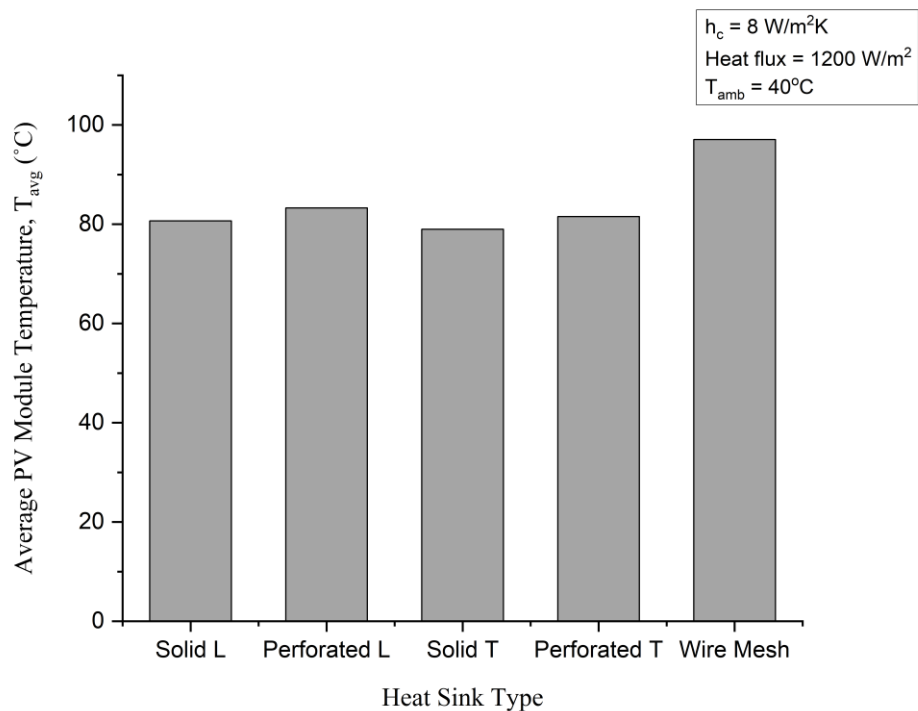


Figure 4.21: Average PV Module Temperature for all Heat Sink Models at fixed values of Convection Coefficient, Heat Flux and Ambient Temperature.

CHAPTER FIVE

CONCLUSION AND RECOMMENDATION

5.1 CONCLUSION

For passively cooling solar panels, five different geometries of aluminium heat sink have been tested under steady state conditions by numerical simulation. The best results are achieved when using Solid T fins arranged in a grid-like pattern over the tedlar surface of the solar panel, where maximum heat dissipation is observed. This particular geometry provides a minimum of 2.08% and a maximum of 18.6% reduction in T_{avg} relative to the other geometries. The findings from the results are summarized as follows:

- T_{avg} increases linearly with increase in solar radiation.
- Both greater solar radiation and T_{amb} result in higher T_{avg}
- At the same value of solar radiation at different values of T_{amb} , T_{avg} is lowest for Solid T fins.
- Solar radiation and T_{amb} have much greater effect than h_c on T_{avg} .
- At higher values of h_c , better cooling effect is observed.
- Solid T fins produce the maximum cooling effect among all five chosen geometries.
- Solid fins produce greater cooling effect than their perforated variants.
- The performance of the wire mesh geometry is significantly worse than the rest of the geometries.
- The temperature distribution on the PV module is dependent on the grid arrangement, as greater cooling effect is seen at the points of contact.
- Using a more concentrated grid of heat sinks will produce better cooling effects, but incur greater material cost.

5.2 RECOMMENDATION AND FUTURE SCOPES

The numerical model in this work assumes perfectly controlled conditions where random environmental variables are neglected, considered constant, or varied in particular increments. This means that the model provides a fair baseline for the solar panel parameters and operating conditions. Therefore, the performance of various other types of heat sink geometries can be assessed by numerical simulation using this same model. Alternatively, the dimensions of the heat sinks used in this study can be optimized further by using data from previous studies to polish the dimensions even further. The results obtained from using the model in this study can be used to determine the feasible heat sink configurations that can be implemented in real life. Hence, using the best performing configurations, experimental work can be performed to find the degree of agreement between the sets of results. Since T_{avg} is most significantly affected by solar radiation and T_{amb} , using these two parameters for comparison can help in establishing clear contrast among various heat sink models. Another scope is to use the same heat sink configurations to test against various specifications of solar panels. One of the assumptions in this study is the consideration of stagnant air around the solar panel, so future work may incorporate the factor of incident wind speed on the heat sinks, which would facilitate the dissipation of heat. This requires some work to be done to figure out equivalent convection coefficients that address the variation of wind velocity. Some of the limitations in this study have been the computational power and time constraint. In the event that none of these constraints are present, transient state simulation can be performed in order to address the time-dependent aspects such as the fluid dynamics and other thermal properties. The results obtained from using the model in this study can be used to determine the feasible heat sink configurations that can be implemented in real life. Hence, using the best performing configurations, experimental work can be performed to find the degree of agreement between the sets of results.

REFERENCE

- [1] Shiva Kumar B, Sudhakar K. Performance evaluation of 10 MW grid connected solar photovoltaic power plant in India. *Energy Reports* 2015;1:184–92. <https://doi.org/10.1016/j.egy.2015.10.001>.
- [2] IRENA. Solar Energy Data. Install Capacit Trends 2019:1–5. <https://www.irena.org/solar>.
- [3] Fesharaki VJ, Dehghani M, Fesharaki JJ, Tavasoli H. The Effect of Temperature on Photovoltaic Cell Efficiency. *Proceeding 1st Int Conf Emerg Trends Energy Conserv* 2011:20–1.
- [4] Siecker J, Kusakana K, Numbi BP. A review of solar photovoltaic systems cooling technologies. *Renew Sustain Energy Rev* 2017;79:192–203. <https://doi.org/10.1016/j.rser.2017.05.053>.
- [5] de Winter F. Solar collectors, energy storage, and materials n.d.
- [6] Bakari R, Minja RJA, Njau KN. Effect of Glass Thickness on Performance of Flat Plate Solar Collectors for Fruits Drying. *J Energy* 2014;2014:1–8. <https://doi.org/10.1155/2014/247287>.
- [7] Badiie A, Ashcroft IA, Wildman RD. The thermo-mechanical degradation of ethylene vinyl acetate used as a solar panel adhesive and encapsulant. *Int J Adhes Adhes* 2016;68:212–8. <https://doi.org/10.1016/j.ijadhadh.2016.03.008>.
- [8] Jiang S, Wang K, Zhang H, Ding Y, Yu Q. Encapsulation of PV Modules Using Ethylene Vinyl Acetate Copolymer as the Encapsulant. *Macromol React Eng* 2015;9:522–9. <https://doi.org/10.1002/mren.201400065>.
- [9] Alaaeddin MH, Sapuan SM, Zuhri MYM, Zainudin ES, Al-Oqla FM. Polyvinyl fluoride (PVF); Its Properties, Applications, and Manufacturing Prospects. *IOP Conf Ser Mater Sci Eng* 2019;538. <https://doi.org/10.1088/1757-899X/538/1/012010>.
- [10] Ebnesajjad S. *Polyvinyl Fluoride: Technology and Applications of PVF*. Elsevier; 2012. <https://doi.org/10.1016/C2011-0-05117-7>.

- [11] Zhang D, Allagui A. Chapter 8 - Fundamentals and performance of solar photovoltaic systems. In: Assad MEH, Rosen MA, editors. *Des. Perform. Optim. Renew. Energy Syst.*, Academic Press; 2021, p. 117–29. <https://doi.org/https://doi.org/10.1016/B978-0-12-821602-6.00009-2>.
- [12] Jiang L, Cui S, Sun P, Wang Y, Yang C. Comparison of Monocrystalline and Polycrystalline Solar Modules. *Proc 2020 IEEE 5th Inf Technol Mechatronics Eng Conf ITOEC 2020* 2020;341–4. <https://doi.org/10.1109/ITOEC49072.2020.9141722>.
- [13] Martin II J. Monocrystalline vs Polycrystalline Solar Panels: Busting Myths 2012. <https://www.solarchoice.net.au/blog/monocrystalline-vs-polycrystalline-solar-panels-busting-myths/>.
- [14] Perraki V. Temperature Dependence on the Photovoltaic Properties of Selected Thin-Film Modules. *Int J Renew Sustain Energy* 2013;2:140. <https://doi.org/10.11648/j.ijrse.20130204.12>.
- [15] Green M, Dunlop E, Hohl-Ebinger J, Yoshita M, Kopidakis N, Hao X. Solar cell efficiency tables (version 57). *Prog Photovoltaics Res Appl* 2021;29:3–15. <https://doi.org/10.1002/pip.3371>.
- [16] Cui Y, Yao H, Hong L, Zhang T, Tang Y, Lin B, et al. 17% efficiency organic photovoltaic cell with superior processability. *Natl Sci Rev* 2019;7. <https://doi.org/10.1093/nsr/nwz200>.
- [17] Gaglia AG, Lykoudis S, Argiriou AA, Balaras CA, Dialynas E. Energy efficiency of PV panels under real outdoor conditions—An experimental assessment in Athens, Greece. *Renew Energy* 2017;101:236–43. <https://doi.org/10.1016/j.renene.2016.08.051>.
- [18] Du D, Darkwa J, Kokogiannakis G. Thermal management systems for Photovoltaics (PV) installations: A critical review. *Sol Energy* 2013;97:238–54. <https://doi.org/10.1016/j.solener.2013.08.018>.
- [19] Atsu D, Seres I, Aghaei M, Farkas I. Analysis of long-term performance and reliability of PV modules under tropical climatic conditions in sub-Saharan. *Renew Energy* 2020;162:285–95. <https://doi.org/10.1016/j.renene.2020.08.021>.

- [20] Bahaidarah HMS, Baloch AAB, Gandhidasan P. Uniform cooling of photovoltaic panels: A review. *Renew Sustain Energy Rev* 2016;57:1520–44. <https://doi.org/10.1016/j.rser.2015.12.064>.
- [21] Barako MT, Park W, Marconnet AM, Asheghi M, Goodson KE. Thermal cycling, mechanical degradation, and the effective figure of merit of a thermoelectric module. *J Electron Mater* 2013;42:372–81. <https://doi.org/10.1007/s11664-012-2366-1>.
- [22] Ndiaye A, Kébé CMF, Charki A, Ndiaye PA, Sambou V, Kobi A. Degradation evaluation of crystalline-silicon photovoltaic modules after a few operation years in a tropical environment. *Sol Energy* 2014;103:70–7. <https://doi.org/10.1016/j.solener.2014.02.006>.
- [23] Kumar M, Kumar A. Performance assessment and degradation analysis of solar photovoltaic technologies: A review. *Renew Sustain Energy Rev* 2017;78:554–87. <https://doi.org/10.1016/j.rser.2017.04.083>.
- [24] Dwivedi P, Sudhakar K, Soni A, Solomin E, Kirpichnikova I. Advanced cooling techniques of P.V. modules: A state of art. *Case Stud Therm Eng* 2020;21:100674. <https://doi.org/10.1016/j.csite.2020.100674>.
- [25] Cuce E, Bali T, Sekucoglu SA. Effects of passive cooling on performance of silicon photovoltaic cells. *Int J Low-Carbon Technol* 2011;6:299–308. <https://doi.org/10.1093/ijlct/ctr018>.
- [26] Gotmare JA, Borkar DS, Hatwar PR. Experimental Investigation of Pv Panel With Fin Cooling Under Natural Convection 2015:447–54.
- [27] El Mays A, Ammar R, Hawa M, Akroush MA, Hachem F, Khaled M, et al. Improving Photovoltaic Panel Using Finned Plate of Aluminum. *Energy Procedia* 2017;119:812–7. <https://doi.org/10.1016/j.egypro.2017.07.103>.
- [28] Bayrak F, Oztop HF, Selimefendigil F. Effects of different fin parameters on temperature and efficiency for cooling of photovoltaic panels under natural convection. *Sol Energy* 2019;188:484–94. <https://doi.org/10.1016/j.solener.2019.06.036>.
- [29] Elbreki AM, Sopian K, Fazlizan A, Ibrahim A. An innovative technique of

- passive cooling PV module using lapping fins and planner reflector. *Case Stud Therm Eng* 2020;19:100607. <https://doi.org/10.1016/j.csite.2020.100607>.
- [30] Arifin Z, Tjahjana DDDP, Hadi S, Rachmanto RA, Setyohandoko G, Sutanto B. Numerical and experimental investigation of air cooling for photovoltaic panels using aluminum heat sinks. *Int J Photoenergy* 2020;2020. <https://doi.org/10.1155/2020/1574274>.
- [31] Popovici CG, Hudişteanu SV, Mateescu TD, Cherecheş NC. Efficiency Improvement of Photovoltaic Panels by Using Air Cooled Heat Sinks. *Energy Procedia* 2016;85:425–32. <https://doi.org/10.1016/j.egypro.2015.12.223>.
- [32] Haque MA, Miah MAK, Hossain S, Rahman MH. Passive cooling configurations for enhancing the photovoltaic efficiency in hot climatic conditions. *J Sol Energy Eng* 2021:1–25. <https://doi.org/10.1115/1.4052062>.
- [33] Salami P, Ajabshirchi Y, Abdollahpoor S, Behfar H. A Comparison Among Different Parameters for the Design of a Photovoltaic/Thermal System Using Computational Fluid Dynamics. *Eng Technol Appl Sci Res* 2016;6:1119–23. <https://doi.org/10.48084/etasr.667>.
- [34] Marinić-Kragić I, Nižetić S, Grubišić-Čabo F, Čoko D. Analysis and optimization of passive cooling approach for free-standing photovoltaic panel: Introduction of slits. *Energy Convers Manag* 2020;204. <https://doi.org/10.1016/j.enconman.2019.112277>.
- [35] Selimefendigil F, Bayrak F, Oztop HF. Experimental analysis and dynamic modeling of a photovoltaic module with porous fins. *Renew Energy* 2018;125:193–205. <https://doi.org/10.1016/j.renene.2018.02.002>.
- [36] Hasan DJ, Farhan AA. Enhancing the efficiency of photovoltaic panel using open-cell copper metal foam fins. *Int J Renew Energy Res* 2019;9:1849–55.
- [37] Kim J, Bae S, Yu Y, Nam Y. Experimental and numerical study on the cooling performance of fins and metal mesh attached on a photovoltaic module. *Energies* 2019;13. <https://doi.org/10.3390/en13010085>.
- [38] Grubišić-Čabo F, Nižetić S, Marinić Kragić I, Čoko D. Further progress in the research of fin-based passive cooling technique for the free-standing silicon

- photovoltaic panels. *Int J Energy Res* 2019;43:3475–95. <https://doi.org/10.1002/er.4489>.
- [39] Devcon. Devcon R2-42 Technical Data Sheet n.d. <https://www.surtime.com/files/F-0022-0004.pdf>.
- [40] SubsTech. Wrought Aluminum Alloy 1100 n.d. https://www.substech.com/dokuwiki/doku.php?id=wrought_aluminum_alloy_1100.
- [41] Hernandez-Perez JG, Carrillo JG, Bassam A, Flota-Banuelos M, Patino-Lopez LD. A new passive PV heatsink design to reduce efficiency losses: A computational and experimental evaluation. *Renew Energy* 2020;147:1209–20. <https://doi.org/10.1016/j.renene.2019.09.088>.
- [42] Daut I, Zainuddin F, Irwan YM, Razliana ARN. Analysis of solar irradiance and solar energy in perlis, northern of peninsular Malaysia. *Energy Procedia* 2012;18:1421–7. <https://doi.org/10.1016/j.egypro.2012.05.158>.